

DTIC FILE COPY

4

David Taylor Research Center

Bethesda, MD 2084-5000

DTRC-90/015 May 1990

Ship Hydromechanics Department
Research and Development Report

AD-A222 492

Measurement of Multiple Blade Rate Unsteady Propeller Forces

by

Stuart D. Jessup

DTRC-90/015 Measurement of Multiple Blade Rate Unsteady Propeller Forces

DTIC
ELECTE
JUN 07 1990
S D D



Approved for public release; distribution is unlimited.

035

MAJOR DTRC TECHNICAL COMPONENTS

- CODE 011 DIRECTOR OF TECHNOLOGY, PLANS AND ASSESSMENT
 - 12 SHIP SYSTEMS INTEGRATION DEPARTMENT
 - 14 SHIP ELECTROMAGNETIC SIGNATURES DEPARTMENT
 - 15 SHIP HYDROMECHANICS DEPARTMENT
 - 16 AVIATION DEPARTMENT
 - 17 SHIP STRUCTURES AND PROTECTION DEPARTMENT
 - 18 COMPUTATION, MATHEMATICS & LOGISTICS DEPARTMENT
 - 19 SHIP ACOUSTICS DEPARTMENT
 - 27 PROPULSION AND AUXILIARY SYSTEMS DEPARTMENT
 - 28 SHIP MATERIALS ENGINEERING DEPARTMENT

DTRC ISSUES THREE TYPES OF REPORTS:

1. **DTRC reports, a formal series**, contain information of permanent technical value. They carry a consecutive numerical identification regardless of their classification or the originating department.
2. **Departmental reports, a semiformal series**, contain information of a preliminary, temporary, or proprietary nature or of limited interest or significance. They carry a departmental alphanumeric identification.
3. **Technical memoranda, an informal series**, contain technical documentation of limited use and interest. They are primarily working papers intended for internal use. They carry an identifying number which indicates their type and the numerical code of the originating department. Any distribution outside DTRC must be approved by the head of the originating department on a case-by-case basis.

UNCLASSIFIED

SECURITY CLASSIFICATION OF THIS PAGE

REPORT DOCUMENTATION PAGE

1a. REPORT SECURITY CLASSIFICATION Unclassified		1b. RESTRICTIVE MARKINGS	
2a. SECURITY CLASSIFICATION AUTHORITY		3. DISTRIBUTION/AVAILABILITY OF REPORT	
2b. DECLASSIFICATION/DOWNGRADING SCHEDULE		Approved for public release; distribution is unlimited.	
4. PERFORMING ORGANIZATION REPORT NUMBER(S) DTRC-90/015		5. MONITORING ORGANIZATION REPORT NUMBER(S)	
6a. NAME OF PERFORMING ORGANIZATION David Taylor Research Center	6b. OFFICE SYMBOL (If applicable) Code 1544	7a. NAME OF MONITORING ORGANIZATION	
6c. ADDRESS (City, State, and ZIP Code) Bethesda, Maryland 20884-5000		7b. ADDRESS (City, State, and ZIP Code)	
8a. NAME OF FUNDING/SPONSORING ORGANIZATION	8b. OFFICE SYMBOL (If applicable)	9. PROCUREMENT INSTRUMENT IDENTIFICATION NUMBER	
8c. ADDRESS (City, State, and ZIP Code)		10. SOURCE OF FUNDING NUMBERS	
		PROGRAM ELEMENT NO. 62323N	PROJECT NO. RB23C22
		TASK NO. 2	WORK UNIT ACCESSION NO.
11. TITLE (Include Security Classification) Measurement of Multiple Blade Rate Unsteady Propeller Forces			
12. PERSONAL AUTHOR(S) Jessup, Stuart D.			
13a. TYPE OF REPORT Final	13b. TIME COVERED FROM _____ TO _____	14. DATE OF REPORT (YEAR, MONTH, DAY) 1990, May	15. PAGE COUNT 61
16. SUPPLEMENTARY NOTATION			
17. COSATI CODES		18. SUBJECT TERMS (Continue on reverse if necessary and identify by block number)	
FIELD	GROUP	SUB-GROUP	
		Marine Propeller, Propeller, Unsteady Loads Bearings Forces, Propeller Loads, Model Experiments	
19. ABSTRACT (Continue on reverse if necessary and identify by block number)			
<p>An experimental investigation of unsteady propeller forces was conducted using model propellers operating in idealized axial wakes. Three-bladed propellers were operated behind 3-, 6-, 9-, and 12-cycle wake screens generating blade rate and multiple axial wake inflow harmonics. The axial wake distributions were measured using a Pitot tube. Unsteady propeller bearing thrust and torque were measured with an unsteady force dynamometer. Measurements were compared to calculations using unsteady propeller lifting surface theory. Also, Laser Doppler Velocimetry (LDV) was used to measure the unsteady flow field about the propeller. LDV measurements were used to evaluate the effect of the propeller on the incoming wake.</p> <p><i>Key words: Unsteady propeller forces, blade rate, multiple axial wake inflow harmonics, Laser Doppler Velocimetry (LDV), unsteady flow field about the propeller.</i></p>			
20. DISTRIBUTION/AVAILABILITY OF ABSTRACT		21. ABSTRACT SECURITY CLASSIFICATION	
<input type="checkbox"/> UNCLASSIFIED/UNLIMITED <input checked="" type="checkbox"/> SAME AS RPT <input type="checkbox"/> DTIC USERS		Unclassified	
22a. NAME OF RESPONSIBLE INDIVIDUAL Stuart D. Jessup		22b. TELEPHONE (Include Area Code) (202) 227-5080	22c. OFFICE SYMBOL Code 1544

CONTENTS

	Page
Notation	v
Abstract	1
Administrative Information	1
Introduction	1
Experimental Technique	2
Propellers, Dynamometry, and Test Facility	2
Screen Generated Wakes	3
Laser Doppler Velocimetry and Effective Wake Measurements	5
Unsteady Force Data Acquisition and Analysis	6
Estimation of Experimental Error	7
Results	7
Unsteady Force Measurements	7
Comparison of Measured Forces With Unsteady Lifting Surface Theory	9
Inflow Wake Decay and its Effect on Force Measurements	10
Effective Wake, Measured Time Average Velocity	11
Effective Wake, Measured Time Dependent Velocity	12
Effective Wake, Calculated Propeller-Induced Velocity	13
Effective Wake, Derived Effective Wake Harmonic	13
Discussion	15
Blade Vibration Associated With 12-Cycle Wake Screen	15
The Role of Effective Wake in Unsteady Force Predictions	16
Conclusions and Recommendations	16
Acknowledgments	17
References	49

FIGURES

1. Propellers tested	18
2. Six-component propeller dynamometer assembly	19
3. Test setup	19
4. Wake screen support	20
5. Wake screens	20
6. Measured nominal wakes generated by screens	21
7. Nominal wake harmonic amplitudes generated by screens	25
8. Test setup showing dynamometer, closed jet test section, and tunnel window insert	25
9. Unsteady thrust measurements	26

FIGURES (Continued)

	Page
10. Volume mean wake harmonic amplitudes for wake screens tested	27
11. Variation of unsteady thrust with harmonic number and reduced frequency.....	28
12. Comparison of calculated and measured unsteady propeller forces	29
13. Decay of six-cycle wake from forward plane to propeller plane	30
14. Decay of nine-cycle wake from forward plane to propeller plane.....	31
15. Reduction of wake harmonic amplitudes due to wake decay from forward pitot tube plane to propeller plane	32
16. Influence of wake amplitude decay on correlation of measured forces with PUF-2 prediction	33
17. Total velocity measurement positions using LDV	34
18. Comparison of LDV measured time average velocity with and without propeller operating at forward plane and propeller plane	35
19. Variation of Total axial velocity with propeller angular position, measured at propeller axial centerline at three positions in the six-cycle wake	36
20. Variation of blade-to-blade propeller induced velocity at various positions in six-cycle wake	37
21. Variation of effective wake axial velocity at propeller plane	38
22. Variation of measured sixth harmonic wake amplitude at propeller plane	39

TABLES

1. Geometry of DTRC model propellers 4119 and 4132	40
2. Harmonic content of axial velocity generated by wake screens, nondimensionalized by volume mean velocity.....	41
3. Unsteady thrust and torque	45

NOTATION

<i>A</i>	Cosine coefficient of Fourier series representing wake velocity distribution
<i>B</i>	Sine coefficient of Fourier series representing wake velocity distribution
<i>C</i>	Total amplitude of Fourier series representing wake velocity distribution
$C(r)_n$	Inflow wake decay factor, reduction of wake harmonic amplitude from $x/R = -0.432$ to $x/R = 0.0$
<i>c</i>	Section chordlength
<i>D</i>	Propeller diameter
<i>EAR</i>	Propeller expanded area ratio
<i>f</i>	Maximum camber of section
<i>J</i>	Advance coefficient, V_{vm}/nD
<i>K</i>	Integer multiple of blade number
K_T	Thrust coefficient, T/n^2D^4
K_Q	Torque coefficient, Q/n^2D^5
<i>k</i>	Reduced frequency
<i>N, n</i>	Harmonic number
<i>n</i>	Propeller rotation speed, revolutions per second
<i>Q</i>	Propeller torque
Q_n	Amplitude of n^{th} harmonic of torque
<i>R</i>	Propeller tip radius
<i>r</i>	Propeller radius
r_h	Propeller hub radius
<i>T</i>	Propeller thrust
T_n	Amplitude of n^{th} harmonic of thrust



Accession For	
NTIS CRA&I	<input checked="" type="checkbox"/>
DTIC TAB	<input type="checkbox"/>
Unannounced	<input type="checkbox"/>
Justification	
By _____	
Distribution/	
Availability Codes	
Dist	Avail and/or Special
A-1	

NOTATION (Continued)

t	Maximum propeller blade section thickness
V_{vm}	Volume mean velocity
\bar{V}_x	Circumferential average axial velocity
$(V_x)_n$	n^{th} harmonic amplitude of V_x
$((V_x)_n)_{vm}$	Volume mean harmonic amplitude of V_x
$V_x(\theta_w)$	Time average axial velocity
$V_x(\theta, \theta_w)$	Axial velocity
x	Axial position, positive downstream, centered at propeller centerline
Z	Propeller blade number
θ	Angular position of propeller, positive clockwise looking upstream referenced to blade centerline.
θ_w	Angular coordinate of wake velocity, positive clockwise looking upstream
θ_b	Blade semichord projected angle
$(\phi_{V_x})_n$	Phase angle of the n^{th} harmonic of axial wake inflow
$(\phi_{T,Q})_n$	Phase angle of the n^{th} harmonic of thrust or torque

ABSTRACT

An experimental investigation of unsteady propeller forces was conducted using model propellers operating in idealized axial wakes. Three-bladed propellers were operated behind 3-, 6-, 9-, and 12-cycle wake screens generating blade rate and multiple axial wake inflow harmonics. The axial wake distributions were measured using a Pitot tube. Unsteady propeller bearing thrust and torque were measured with an unsteady force dynamometer. Measurements were compared to calculations using unsteady propeller lifting surface theory. Also, Laser Doppler Velocimetry (LDV) was used to measure the unsteady flow field about the propeller. LDV measurements were used to evaluate the effect of the propeller on the incoming wake.

ADMINISTRATIVE INFORMATION

The work reported herein was funded by the 6.2 Submarine and Surface Ship Propulsor Exploratory Development Program under the Submarine Technology Program Element 62323N, Project RB23C22, Task 2. The work was performed at the David Taylor Research Center (DTRC) under DTRC Work Unit 1540-005.

INTRODUCTION

In past years the subject of unsteady propeller forces has received continuing effort at DTRC. Marine propellers operate in either the nonuniform wake of a submarine or merchant ship or in inclined flow under the stern of Naval surface ship combatants. In all cases the propeller operates in a spatially nonuniform flow field which develops unsteady periodic blade loading. Because of the periodic nature of propeller rotation, the propeller inflow is treated in a cylindrical coordinate system and is represented by a Fourier or harmonic series with respect to the propeller shaft axis. The wake is characterized by harmonic amplitudes and phases of the three components of velocity at various radial locations. To date most studies have addressed the response of the propeller to the fundamental wake harmonic which is the harmonic associated with the blade number of the propeller. This study will address the propeller response to multiples of the fundamental blade rate wake harmonic.

The operation of a propeller in a nonuniform inflow causes a fluctuation in the angle of attack of the blade sections resulting in alternating blade loads. The net load transmitted to the hub and shaft of the propeller is the sum of the periodic forces generated on the blades. Because of the symmetrical positioning of the blades on the hub, the harmonic content of the blade loads is canceled out or summed when transmitted to net hub or shaft loads. Therefore, unsteady shaft thrust and torque can be generated only by blade rate or multiples of blade rate inflow wake harmonics (KZ). Side forces and moments transferred to the hub are produced by wake harmonic numbers adjacent to blade frequency ($KZ \pm 1$). The unsteady blade loads are filtered by blade number when summed at the hub. This study will address the net hub or shaft forces and not the individual blade loads.

A landmark experimental study of the subject was reported by Boswell and Miller.¹ Six components of unsteady propeller bearing forces were measured on a variety of model propellers tested in the DTRC 24-inch water tunnel operating behind screen-generated axial wake harmonics. These tests utilized blade rate harmonic excitation, for example, three-cycle wake screens and three-bladed propellers.

The goal of unsteady propeller force study is to acquire sufficient understanding of unsteady propeller hydrodynamics to make accurate predictions. Boswell and Miller¹ exercised calculation procedures with varying degrees of success. A more recent study by Boswell² summarizes a variety of calculation procedures for the prediction of hub and blade loads. Present access to high speed computers led to the recommendation that unsteady lifting surface procedures be used to predict unsteady propeller forces. Two of these methods are used at DTRC, those of Kerwin³ and Tsakonas.⁴ These methods utilize distributed singularities along the meanlines of the blade and incorporate various wake models downstream of the blades.

An aspect of the problem that may be important in the prediction of unsteady propeller forces is the influence of the propeller on the incoming flow field. For steady propeller hydrodynamics, this is referred to as the effective wake, which has been defined as the total inflow velocity minus the irrotational propeller-induced velocity as described by Huang.⁵ The method of Huang⁵ has been used to correct typical circumferential average nominal wakes to arrive at an effective wake, but generally no correction is made for the spatially-varying nominal wake harmonics. Methods have been proposed by Van Houten in a paper with Breslin.⁶ The effective wake problem is far from solved and is presently an active area of research.

As part of this study, velocity measurements were made using Laser Doppler Velocimetry with and without the propeller operating in an idealized nonuniform wake field. From these measurements, effective wake harmonics were derived for comparison with the nominal wake.

EXPERIMENTAL TECHNIQUE

PROPELLERS, DYNAMOMETRY, AND TEST FACILITY

Two existing 12-inch model propellers were chosen for this study, DTRC Model Propellers 4119 and 4132. These propellers were designed and manufactured for the original tests of Boswell and Miller.¹ Propeller 4119 is actually a double thick version of Propeller 4118, which was tested by Boswell and Miller.¹ Because Propeller 4118 was not available, 4119 was used in its place. Both propellers have three blades, no skew, and represent typical marine propeller geometry. Propellers 4119 and 4132 have expanded area ratios of 0.6 and 0.3. The propeller geometries are shown in Fig. 1 and tabulated in Table 1. The propellers were operated at their design condition of $J = 0.833$ and run at 10 RPS throughout the test program.

The DTRC 24-Inch Variable Pressure Water Tunnel was used to conduct the tests to be described. The tunnel has a 24-in. diameter open-jet test section. For the measurement of unsteady propeller shaft forces, the 6-component unsteady propeller dynamometer originally developed for the earlier tests¹ was used. A schematic of the dynamometer system is shown in Fig. 2. The

dynamometer incorporates a massive tail shaft coupled to the tunnel and main shaft through flexible soft mounts. This arrangement creates a very low frequency resonant system at around 7 Hz, which is below the frequency range of interest. Attached to the end of the tail shaft is a semiconductor strain-gauged flexure. The flexure produces the upper limit of frequency response of the measurement system at around 800 Hz in thrust and torque and around 200 Hz for the side force components. Further description of the measurement system was given by Miller.⁷

To limit the scope of this study, only unsteady thrust and torque were measured. These forces are the most important and the simplest to measure. Measurement of the side forces and moments is difficult because of the inherent large interactions among the four components. All four channels must be operating equally well and must be calibrated very carefully, paying proper attention to sign conventions. Also, inclusion of side forces would double the test matrix, since the harmonic wake numbers associated with side forces are different from those of thrust and torque.

The configuration of the test section incorporated a closed jet test section that was installed within the existing open jet test section. This set-up was used in the past for the earlier unsteady force studies¹ and for general cavitation tests in which wake screens were used to simulate a specified wake. The closed jet installation involved removing the existing upstream jet nozzles and attaching the wake screen and the cylindrical closed jet sections. With the closed jet installed, the actual test section diameter is increased from 24 in. to 27 in., as shown in Fig. 3.

SCREEN GENERATED WAKES

Wire mesh screens were used to generate the various propeller inflow wake harmonics. This technique was an extension of that used in Boswell and Miller's tests.¹ In their experiments a relatively thin wire mesh base screen spanned the 27-in.-diameter test section approximately 30 in. upstream of the propeller. The base screen (16 per inch \times 0.009 in.) was stretched and soldered on to a steel support ring. Superimposed over the base screen were sections of a coarser screening that were spot welded to the base screen. The screen assembly with support ring was attached to a screen support fixture that supported the screen with numerous radial and circumferential struts approximately 0.125 in. \times 1.5 in. in size.

The support fixture structurally supported the screen and allowed the screen to be rotated. Rotation of the screen permitted the nonuniform wake to be rotated with respect to the tunnel. This feature was potentially valuable for LDV measurements in which the measuring point of the LDV system could remain fixed and the wake could be rotated. This rotation of screen would allow simple axial and tangential velocity surveys to be conducted without use of the more difficult on-axis LDV measurement component. This arrangement requires precise positioning of the propeller at the center axis of the wake. Unfortunately, the 6-component dynamometer did not place the propeller at the tunnel center accurately enough to provide a rotationally independent harmonic wake structure. The screen support is shown in Fig. 4.

The screens used for the present set of experiments incorporated 3-, 6-, 9-, and 12-cycle configurations. The 3-cycle screen was similar to that used in the earlier experiments.¹ The remaining screens were made for the present tests. Figure 5 shows the four screens used. The coarse screen covered half of the base screen area with a 1/16-in. \times 0.018-in. mesh for the 6-, 9-, and 12-cycle screens. The 3-cycle screen incorporated a third screen in an attempt to create a more sinusoidal wake pattern.

The nominal wakes generated by the screens were measured with a Pitot tube without the propeller present. A single United Sensor 0.125-in. diameter Pitot-static tube was mounted on a special hub that replaced the propeller. Circumferential axial velocity surveys were performed at the 0.3, 0.5, 0.7, and 0.9 fraction of propeller tip radius. Surveys were conducted by slowly rotating the propeller shaft and determining the differential pressure across the Pitot tube and the shaft angular position using a 12-bit absolute positioning rotary encoder. For each run the shaft and probe were rotated approximately four revolutions, providing about 120 individual pressure readings at each of 4096 angular positions per revolution. The data were then analyzed by sorting all the individual measurements into the appropriate angular bin, converting each individual pressure measurement into velocity, and averaging the velocity for each bin. This high resolution data acquisition procedure was a modification of a previously developed program for LDV shaft encoded data acquisition.⁸ The high resolution of the shaft position was later averaged to 512 readings per revolution for plotting purposes. Note that the Pitot tube probe was not incremented to allow the pressure to reach a steady value during data collection. At a shaft rotation time of 2 minutes per revolution the probe appeared to respond fast enough to compare well with measurements performed with the LDV system.

The surveys were performed with the 6-component dynamometer in place. Because of this dynamometer configuration, the axial position of the Pitot tube probe was located 2.59 in. upstream of the propeller plane, at $x/R = -0.432$. The flow variation produced by the screens should decay by the square root of the distance downstream. The decay of the harmonic wakes was checked with LDV measurements at the Pitot tube plane and at the propeller plane and will be discussed later. The LDV system was not used for the nominal wake measurements because of the dummy hub blockage of the measurement beams and the lack of automated LDV traverse at the time of the test.

The measured axial wakes for the various screen configurations are shown in Fig. 6. The obvious characteristic of the screen wakes is the decay in the amplitude of the fundamental harmonic with decreasing radius. This trend was also found by Boswell and Miller,¹ but the degree of decay appears to increase with increasing harmonic number of the fundamental. The increasing decay with decreasing radius makes intuitive sense when one observes the geometry of the screens in Fig. 5. The width between shear layers generated by the screens decreases as the radius decreases. As axial distance from the screens increases, the turbulent mixing occurring between layers broadens so that at the inner radii complete mixing occurs close to the screen. This phenomenon is inherent in any simple screen that places the entire screen equidistant from the propeller. A more complex screen may produce a more uniform harmonic amplitude with radius, but experience has shown that a simpler screen configuration is more

predictable. The goal of the project was not necessarily generation of radially uniform wake amplitudes, but constant measurable wakes, with large enough amplitudes to produce measurable response.

For prediction of the measured unsteady propeller forces the measured axial wakes were analyzed harmonically. The harmonic coefficients, amplitudes, and phases are listed in Table 2. Figure 7 shows the variation of the various harmonic amplitudes with radius. The wake data can be characterized as follows:

$$V_x(\theta_w)/V_{vm} = \bar{V}_x/V_{vm} + \sum_{n=1}^{15} \{(V_x)_n/V_{vm} \cos[n\theta_w - (\phi_{V_x})_n]\}.$$

From Table 3,

$$V_x(\theta_w)/V_{vm} = MEAN + \sum_{N=1}^{15} \{C \cos[N\theta_w - (PHASE)_N]\},$$

or

$$V_x(\theta_w)/V_{vm} = \sum_{N=1}^{15} (A \cos N\theta_w + B \sin N\theta_w),$$

where

$$MEAN = \bar{V}_x/V_{vm}$$

$$C = (V_x)_n/V_{vm}$$

$$V_{vm} = \frac{2}{(R^2 - r_h^2)} \int_{r_h}^R V_x r dr, \text{ volume mean velocity}$$

$$\theta_w = \text{angle about propeller axis, positive clockwise looking upstream}$$

$$PHASE, (\phi_{V_x})_n = \text{phase angle of the } n^{\text{th}} \text{ harmonic of axial wake inflow.}$$

LASER DOPPLER VELOCIMETRY AND EFFECTIVE WAKE MEASUREMENT

A Laser Doppler Velocimetry (LDV) system was used to measure the total axial velocity near the propeller while it was operating. The LDV system consisted of a one-component, on-axis backscatter dual beam configuration with beam expansion and a 250-mm focusing lens. A tunnel window insert was used in the open jet test section to move the optics closer to the measurement point. A modified section of the closed-jet nozzle was constructed to accommodate the

tunnel window insert. Figure 8 shows this modification along with the 6-component dynamometer. The relatively short focal length optical system produced a small measuring point (0.003-in. diameter). LDV velocity measurements were collected along with simultaneous measurement of the angular position of the propeller shaft. Velocity measurements were later sorted by blade angular position so that the variation of the flow with blade position could be obtained. Further description of the LDV system, data acquisition, and analysis is given in an earlier paper.⁸

With the LDV, axial velocity versus blade position was measured while the propeller was in operation. Measurements were made at two axial planes, one corresponding to the location of the Pitot tube measurements at $x/R = -0.432$, and one corresponding to the propeller axial centerline, $x/R = 0.0$. Measurements were made with Propeller 4132 operating behind only the 6-cycle wake screen, at the 0.5, 0.7, and 0.9 fraction of tip radius. Individual measurement runs were made at 2.5-degree increments from -30 to $+30$ degrees from the horizontal plane. This series of measurements defined the flow through one harmonic cycle of the 6-cycle screen wake. Because of practical constraints of shaft blockage, insufficient traversing range, and manual traversing, the entire propeller plane was not measured. On the assumption that the wake had a 6-cycle period, the measurement matrix was sufficient. Detailed data will be presented in this report at only the 0.7 radius.

Limited time-averaged wake measurements were made using the LDV system. Measurements were made with and without the propeller operating at selected radii for the 6- and 9-cycle wake screens. Measurements of velocity were read directly from the LDV tracker processor through one wake cycle. These measurements provided a check against the Pitot tube results and provided information on the wake decay from the forward Pitot tube plane to the propeller plane.

UNSTEADY FORCE DATA ACQUISITION AND ANALYSIS

Unsteady thrust and torque data were collected using two techniques. The first method utilized an Interdata model 70 type minicomputer and an incremental, 90-pulse/revolution encoder mounted on the propeller shaft. Thrust and torque data were collected every 4 degrees, 90 times per revolution for 300 revolutions, and stored on 9-track digital tape. The data were analyzed by averaging the 300 force measurements at each angular position. The interaction of torque on thrust was then corrected and a harmonic analysis was performed on thrust and torque. Data were collected at a design advance coefficient of 0.833 and a shaft rotation speed of 10 RPS.

The second method of data collection utilized modification of the LDV data acquisition system. Thrust and torque measurements were triggered randomly by the LDV tracker processor with the LDV system running. Simultaneously, the shaft position was also recorded with an absolute positioning 12-bit resolution (4096/rev) shaft encoder. Later the data were sorted by angular position with a resolution of 4096 per revolution. This method provided a check on the first data acquisition method and provided higher angular resolution. Harmonic analysis was performed on the force signals and the results correlated with those of the first method to within 2%.

ESTIMATION OF EXPERIMENTAL ERROR

Estimates were made of the accuracy of the measured test quantities based on uncertainties in the general test configuration and the estimated accuracy of the individual test quantity.

- Velocity measurements, $\pm 0.01 V_{vm}$ (including LDV, Pitot measurements, and measured wake harmonics)
- Thrust and torque measurements, $\pm 0.01 (T, Q)_o$ (including amplitude of force harmonics)
- Propeller operating conditions, ± 1 RPM, $\pm 0.01 J$

RESULTS

UNSTEADY FORCE MEASUREMENTS

Unsteady thrust and torque measurements were made for Propellers 4132 and 4119 operating at design $J=0.833$ behind the 3-, 6-, 9-, and 12-cycle wake screens. The unsteady thrust response for the propellers operating behind the 9-cycle screen is shown in Fig. 9a. The propellers responded to the primary 9th harmonic of the axial inflow wake and produced a variation in thrust nine times per revolution (9th harmonic).

Propeller 4119 also showed a high frequency response at around the 78th harmonic corresponding to a frequency of 780 Hz and is probably associated with the axial resonance of the dynamometer at 800 Hz. Oddly, the phase averaging effect of the data acquisition procedure did not average out the presumed random vibration due to the axial resonance. This high frequency response is isolated enough from the primary 9th harmonic response to indicate that it has no effect on the results of interest.

The harmonic amplitudes from the harmonic analysis of the thrust variation with shaft rotation are also shown in Fig. 9a. The 9th harmonic is dominant due to the dominant 9th harmonic of the wake, which is tabulated in Table 2. Also seen are significant amplitudes at the 1st, 3rd, and 6th harmonic. The first harmonic has been observed in previous experiments¹ and is generally attributed to misalignments of the propeller to the axial center of the incoming wake or to asymmetry of the propeller blades about the axis of rotation. The first harmonic response is considered unimportant, that is, it does not significantly affect the higher harmonics of interest. The 3rd and 6th harmonic responses are partially due to some 3rd and 6th harmonic content in the inflow wake. There may be some nonlinear interaction between harmonic responses that causes harmonic response at fractions of the fundamental wake harmonic. These effects are little understood and are not thought to be significant in the lifting surface theory.^{3,4} The primary interest in this study is the prediction of the primary wake response, in this case the 9th harmonic.

Also shown in Fig. 9a is the smaller response of the wider-bladed Propeller 4119 to the 9th harmonic wake. Simply, the reduced response is due to load cancellation that occurs chordwise over the blade. This effect is characterized by the nondimensional parameter k , the reduced frequency, which for a propeller is closely approximated by $n\theta_b$, the product of the harmonic number and the projection of the blade semichord onto the propeller plane. The reduced frequency is a measure of the unsteadiness of the flow. At low reduced

frequency the unsteady effects are small and the assumption of a quasi-steady flow is valid; at high reduced frequency, unsteady effects become large and tend to reduce the loading response from a quasi-steady analysis.¹ Because Propeller 4119 has chord lengths twice those of Propeller 4132, its characteristic reduced frequency is twice as large, and greater unsteady effects tend to reduce loading response.

The load response of the two propellers tested in the various wakes is qualitatively similar to that shown in Fig. 9a. Generally, torque behaves in much the same way as thrust. Tabulations of the measured thrust and torque response are presented in Table 3. Included in these tables are calculated responses, which will be discussed later. The tabulated data represent the thrust and torque loading as a Fourier series in blade angular position in the following form:

$$\text{Thrust, } T(\theta), \text{ Torque, } Q(\theta) = (T, Q)_{n=0} + \sum_{n=1}^{15} (T, Q)_n \cos(n\theta - (\phi_{T, Q})_n)$$

where $(T, Q)_{n=0}$ = circumferential average value of T, Q

$(T, Q)_n$ = amplitude of the n^{th} harmonic of T, Q

θ = angular position in the propeller disk, positive clockwise looking upstream (right handed propeller) in degrees

$(\phi_{T, Q})_n$ = phase angle of n^{th} harmonic of T, Q where the reference line is the blade reference line, in degrees.

All thrust and torque quantities are represented nondimensionally as thrust and torque coefficients, K_T and K_Q . Figure 9b shows the harmonic amplitude of thrust for each propeller operating in the wake of the screens tested. The reduction of response with increasing screen cycle is obvious. This effect is partially due to the reduction in the produced wake harmonics with increasing screen cycles.

The response of the propellers to the various wakes also demonstrates the effect of reduced frequency. To make consistent comparisons of the loading response for the various screens, the response must be normalized by a representative magnitude of the exciting inflow wake harmonic. Normalization is necessary because of the decrease in primary wake amplitudes generated by the screens when the screen cycle number increases, as is shown in Fig. 7. Therefore, a volume mean wake harmonic amplitude was calculated as follows to represent an average primary wake harmonic amplitude for each screen:

$$((V_x)_n)_{vm} = \frac{2}{(R^2 - r_h^2)} \int_{r_h}^R (V_x)_n r dr.$$

The resulting volume-mean wake harmonic amplitude for the various screens is shown in Fig. 10. The integration of the exciting wake harmonic amplitude is reasonable in this case because the phase of the primary wake

harmonic amplitude is constant over the radius, and the propellers tested have the same skew distribution (i.e., constant, no skew). As expected, the volume mean wake harmonic amplitude decreases with increasing screen cycle number. These values were then used to normalize the measured loading response for consistent comparison. Figure 11 shows the variation of normalized loading with the primary harmonic number of each screen and the reduced frequency. The top plot shows a greater response of the narrow-bladed propeller at higher screen number, but when the propellers are compared in terms of reduced frequency, the normalized responses are similar. At low reduced frequency the wide-bladed propeller shows a larger response due to its longer chord length, which results in larger quasi-steady lift. In later comparisons with unsteady lifting surface theory, this low reduced frequency effect is also properly represented.

COMPARISON OF MEASURED FORCES WITH UNSTEADY LIFTING SURFACE THEORY

The goal of this study was to improve the ability to predict unsteady propeller bearing forces occurring at multiples of blade rate. Therefore, the measured forces were predicted, using the unsteady lifting surface theory code PUF-2,³ and were compared with measured data.

PUF-2 calculations were performed for both Propellers 4132 and 4119 using the measured nominal wake as shown in Fig. 6 and tabulated in Table 2. The resulting calculated unsteady thrust and torque are tabulated in Table 3 to show the calculated response at blade rate and its multiples for the various screen wakes. Also listed in Table 3 is the ratio of the calculated to measured amplitudes and the difference in the calculated and measured phase angles. Figure 12 plots the comparison of the measured and calculated harmonic amplitudes and phases of the primary wake harmonic for each screen configuration. If the calculation were to match the measured result exactly, then the ratio of the amplitudes would be one and the difference in the phases would be zero.

Figure 12 also shows a calculated comparison with and without the modeling of propeller wake vorticity attenuation. During early evaluation of PUF-2, correlation with other methods showed lower blade rate calculation amplitudes than other methods for a sample four-bladed propeller. PUF-2 models the propeller's downstream wake with vortex lattice elements distributed within a transition wake region. After a prescribed angular passage of the propeller, typically 90 degrees, the inner wake converges to a hub vortex and the outer wake converges to a tip vortex, at the roll-up point. The vortex sheet, shed because of the unsteady lift, when convected to the roll-up point, causes a discontinuity in the wake model which causes large inductions on the adjacent blade. To reduce the unrealistic effect, the shed vorticity was allowed to attenuate from the trailing edge of the blade to the roll-up point. Thus, attenuating the shed vortex wake will reduce the unsteady effects on the blade lift variation and should therefore increase the unsteady loading. PUF-2 calculations with and without wake vorticity attenuation can show sensitivity of the calculated loadings to details of the downstream wake model.

Generally, PUF-2 tends to over-predict the measured loads, except for the 12-cycle wake. The prediction for the 3-cycle wake is close but it increasingly over-predicts for the 6- and 9-cycle wakes and then decreases for the 12-cycle wake. Modeling wake vorticity attenuation tended to increase the predictions, contrary to previous experience with a four-bladed propeller. The over-prediction may have been due to the effect of the three-bladed propeller run with a 90-degree angular extent of the roll-up point. It does appear that better correlation occurred without vortex wake decay.

INFLOW WAKE DECAY AND ITS EFFECT ON FORCE PREDICTIONS

These calculations of the measured unsteady forces were performed using wake measurements made with Pitot tubes positioned forward of the propeller at $x/R = -0.432$. Again this arrangement was necessitated by the practical constraints of conducting the wake surveys with the 6-component dynamometer and drive installed in the tunnel. Partial wake surveys were made using the LDV system at the Pitot tube plane and the propeller plane to estimate the change in inflow wake or inflow wake decay between $X/R = -0.432$ and 0.0 in the absence of the propeller. Initially it was believed that the effect of nominal wake decay was small, so that measured and calculated forces were correlated using the Pitot tube wake directly. In the course of this investigation, study of the decay of the wake showed a significant reduction in the measured Pitot tube wake amplitudes from the Pitot tube plane to the propeller plane. For convenience, the original calculations have been retained but have been supplemented with additional calculations and a best estimate of the wake at the propeller plane in the absence of the propeller.

Using the LDV system, nominal wake measurements were made at the Pitot tube measurement plane, $x/R = -0.423$ and the propeller plane, $x/R = 0.0$. These measurements were made at 2.5-degree increments over a limited extent of the propeller disk, typically 60 degrees. Measurements were made at the 0.5 and 0.7 radius of the 6-cycle screen and 0.7 and 0.9 radius of the 9-cycle screen. Because it was not possible to measure the entire disk, these data are approximate, since effects observed in the measurement of one harmonic cycle are extrapolated to occur on all other cycles in the complete revolution.

Figures 13 and 14 show the results of the LDV surveys at the two planes for the 6- and 9-cycle screen wakes. From the measured results, a significant reduction in the overall variation in the wake can be seen. To quantify the magnitude of the reduction of the primary wake harmonic, the measured data were harmonically analyzed. Shown in Figs. 13 and 14 is the reconstruction of the measured wake using the first four harmonics of the fundamental to verify a reasonable representation of the measured result. From this, a multiplicative reduction factor $C(r)_n$ was obtained by the ratio of the magnitude of the fundamental wake harmonic amplitudes at the two planes.

$$C(r)_n = \frac{\{(V_x)_n\}_{x/R = 0.0}}{\{(V_x)_n\}_{x/R = -0.432}} \quad (\text{LDV, Partial Disk Survey})$$

The reduction factors obtained were then applied to the Pitot tube measured nominal wake harmonics.

$$[(V_x)_n]_{x/R = 0.0} = C(r)_n [(V_x)_n]_{x/R = -0.432} \quad (\text{Pitot, Full Disk Survey})$$

The effect of the wake decay is shown in Fig. 15 for the 6- and 9-cycle primary wake harmonic amplitudes. Figure 15 indicates that the wake decay is approximately constant with radius. This is consistent with the observed general reduction of wake harmonic amplitudes at the inner radii. Therefore, the inflow wake decay was assumed to be constant over radius, reducing the Pitot tube wake harmonic amplitudes by approximately $(V_x)_n/V_{vm} = 0.022$ at the propeller plane. There was no significant change in the phase of the harmonic amplitudes due to wake decay.

The unsteady forces predicted by PUF-2 were recalculated using the Pitot tube results as shown in Table 2 but with the primary wake harmonic amplitudes decreased by 0.022. These results are shown in Fig. 16 in which the original calculations (with wake vorticity attenuation) are compared with calculations including wake corrections. All cases except the 12th harmonic wake show an improvement in the predictions relative to the measured data. Propeller 4119 still shows an overprediction but Propeller 4132 is very close.

Two significant effects would hypothetically improve the correlation between theory and experiment. The first is the influence of the propeller on the incoming nominal wake. This topic was studied using the LDV measurements and will be addressed next in this report. The second is the effect of blade resonant vibration in amplifying the measured responses, which will be addressed in the discussion section of this report.

EFFECTIVE WAKE, MEASURED TIME AVERAGE VELOCITY

The LDV system was used to measure the total velocity with the propeller operating at the forward Pitot tube measurement plane ($x/R = -0.432$) and at the propeller plane ($x/R = 0.0$). Because the measurements were so time consuming, surveys were restricted to Propeller 4132 operating in the 6-cycle wake screen, measuring at the 0.7 radius. This permitted a measurement of almost one full cycle of the sixth wake harmonic, which varies circumferentially plus and minus 30 degrees from the reference horizontal position, as shown in Fig. 17.

The simplest comparison of the harmonic wake with and without the operating propeller is performed using the measured time-averaged velocity. The nominal wake LDV measurements were made at the forward and propeller planes as shown in Fig. 13. The total velocity, with the propeller operating, is compared to the nominal wakes in Fig. 18. In the plane of the propeller, at $x/R = 0.0$, the time-averaged total velocity becomes contaminated by blade passage through the LDV measuring volume and requires a time average derived from measurements obtained with respect to the propeller angular position, which will be discussed later.

It is clear from Fig. 18 that the effect of the propeller is much larger at the propeller plane than at the upstream Pitot tube plane. Qualitatively, it appears that the sixth harmonic amplitude is reduced by propeller operation, with a

larger reduction at the propeller plane. This effect must be further evaluated by removing the included propeller-induced velocities that may vary circumferentially through the wake. Also, the variation in the harmonic wake structure with propeller operation may influence the resulting unsteady blade loading.

EFFECTIVE WAKE, MEASURED TIME DEPENDENT VELOCITY

The intention of the study was to look at a particular wake-propeller configuration in great detail to evaluate the various effects of the propeller on the incoming wake. The propeller plane was chosen for detailed study because the propeller effects and blade loads are largest there. Also, most propeller analysis programs use wake data at the propeller plane for calculations.

Time varying LDV measurements were made at the locations shown in Fig. 17 in the propeller plane during rotation, twenty-two individual data collections runs were made from θ_w equal to -25 degrees to $+27.5$ degrees at 2.5-degree increments at the 0.7 radius with Propeller 4132 operating behind the 6-cycle wake screen. Each data run was reduced to velocity measurements at each of 512 positions in one revolution of the propeller, with each measurement representing an average of approximately 100 individual measurements per angular position. Figure 19 shows the variation of the measured total velocity with propeller angular position for three locations in the circumferentially varying wake. Three distributions are shown, two at the high velocity region of the wake (at θ_w equal to -25 and 27.5 degrees) and one in the low velocity region of the wake (at θ_w equal to 0 degrees). Figure 19a shows the flow variation for one complete revolution of the propeller. The flow has a period of one-third revolution, 120 degrees, generated by the three blades of the propeller. Generally, the axial velocity is minimum in the region between the blades and maximum near the suction side of the blades, which is to the right of the blade passage points. At θ_w equal to 0 degrees, where the nominal velocity is minimum and blade loading is highest, the total velocity is also lowest between the blades but rises as high as at the other wake positions near the suction side of the blade. The difference in velocity squared between the suction and pressure sides of the blades will be proportional to the blade loading.

Figure 19b shows the details of the blockage of the LDV laser beams due to blade passage, when the blades block the LDV laser beams and interrupt the measurement process. There is a narrow band at each blade passage where measurement is interrupted by the finite thickness of the blades, representing a real flow effect due to blade thickness. Blockages also occur when the measuring point is moved vertically up and down. When moving up to measure at positive θ_w angles, the beams are blocked from the pressure side of the blade and, when moving down to negative θ_w angles, the suction side is blocked. This blockage causes some biasing near the blade surfaces when profile averages are calculated. Because of the blockage problem, details near the blade surfaces will be addressed only qualitatively.

Figure 19c shows details of the velocity profiles during blade passage. The general effect of the inflow wake and blade loading can be seen in more detail. This figure shows a real flow effect on the harmonic inflow. A substantial drop in velocity can be seen at the suction side surface. This drop can be attributed

to the suction side blade boundary layer. The pressure side boundary layer should produce a similar drop in velocity near the pressure side blade surface, but it is not seen in these profiles, perhaps due to blade blockage. Increasing the thickness of the blade boundary layer will tend to reduce the peak in velocity near the suction side of the blade and will influence the induction effect of the propeller on the flow. In the actual flow the blade boundary layer is unsteady and the boundary layer thickness fluctuates with the loading on the blade. Therefore a fluctuating variation in the peak velocity would occur near the suction side of the blade, causing a reduction in the harmonic wake inflow. This observation points to the general effect of unsteady blade boundary layer growth on propeller performance in nonuniform inflows. Two-dimensional unsteady boundary layer calculations could provide some insight on the magnitude of this effect compared to more global effects of the propeller on the incoming flow vorticity.

EFFECTIVE WAKE, CALCULATED PROPELLER INDUCED VELOCITY

The effective wake is derived by subtracting the propeller-induced velocity from the total measured velocity. Presently, the propeller-induced velocity can be calculated from potential flow lifting surface theory.³ To investigate the effective wake in detail the potential flow calculation included the circumferential variation of the propeller induction as modeled in the lifting surface code PUF-2. This same code was used for the unsteady force calculations.

Field point velocity calculations were made using PUF-2 for Propeller 4132 operating behind the 6-cycle screen represented by the nominal wake in Table 2. Field points were calculated at the propeller centerline and output was interpolated to the 0.7 radius. Figure 20 shows the calculated propeller-induced axial velocity for various circumferential positions in the wake. Note that the phase of each velocity distribution has been shifted by the angular location in the wake, representing the propeller induction from the moving blade frame of reference. At θ_w equal to 0 the nominal wake is a minimum and the blade loading is approximately a maximum, resulting in a maximum induced velocity near the suction side of the blade and a minimum induced velocity near the pressure side of the blade. At θ_w equal to plus or minus 30 degrees the nominal wake is a maximum and the loading is approximately minimum so that the blade suction side induced velocity is a minimum and the blade pressure side induced velocity is a maximum.

An interesting aspect of the unsteady induced velocity field is the null point that occurs at around 70 degrees (see Fig. 20). For this case of a propeller operating in a harmonic wake field that is a multiple of the propeller blade number, there exists a point between the blades, moving with the blades, at which the induced velocity is constant. A wake measurement at the null point, moving with the blades, would require no adjustment for the effect of the propulsor on the wake harmonic. This phenomenon is probably not generally true for wake harmonics that are not multiples of blade number.

EFFECTIVE WAKE, DERIVED EFFECTIVE WAKE HARMONIC

From the calculations shown in Fig. 20, an effective wake harmonic was derived. First, the calculated induced velocities were interpolated to the

measured circumferential wake positions. Then the calculated profiles were subtracted from the measured profiles summarized in Fig. 19. Figure 21 shows the resulting effective wake profiles verses blade angular position relative to spatial wake position, $\theta - \theta_w$. Profiles are shown for each position θ_w through the sixth-cycle wake. Also shown are vertical bands indicating the areas near the blade surfaces where the analysis should be ignored. If the variation in measured total velocity shown in Fig. 19 was due entirely to potential flow effects properly accounted for in PUF-2, then the profiles shown in Fig. 21 would be constant with angle or straight horizontal lines. This is generally not the case especially near the suction side of the blade which implies that either the potential flow model is incorrect in this region or an additional viscous or rotational effect is present.

A final representation of the effective wake harmonic was made by performing a harmonic analysis at each angular position between the blades. This analysis used the effective wake variation with wake position θ_w for each relative propeller angular position $\theta - \theta_w$. The harmonic analysis was performed over only one cycle of the sixth harmonic wake. Also, velocity values at the extremities of the wake cycle, i.e., $\theta_w = 27.5$ and -30 degrees, were approximated by using the measured adjacent values.

The derived sixth harmonic wake amplitude through one blade passage is shown in Fig. 22. The regions contaminated by blade thickness and beam blockage are indicated with vertical bars at the edges of the blade passage. Three harmonic amplitude distributions are shown. The first is the harmonic amplitude derived from the measured total velocity with no removal of the effects of the propeller. The second distribution is the total velocity with the propeller-induced velocities, as shown in Fig. 21, subtracted to give the effective harmonic amplitude. The propeller-induced velocities used for this case were calculated using the nominal wake harmonic amplitudes measured at the upstream plane using the Pitot tube. This wake was estimated to be high due to the wake decay from the upstream plane to the propeller plane. The second distribution was derived using a reduced variation in propeller-induced velocities calculated with input wake amplitudes reduced by 12% from the first distribution. The second distribution represents an approximate calculation using the correct estimated wake at the propeller plane.

The harmonic amplitudes derived from the total velocity can be compared with the two effective velocity distributions. All three curves converge at the null point between the blades where the propeller-induced velocity is independent of the blade position in the wake, as discussed earlier with respect to Fig. 20. An account of the propeller-induced velocity tends to make the blade-to-blade distribution of the harmonic amplitude more nearly constant than consideration of only total velocity. As discussed earlier, if the unsteady flow field were completely irrotational, then the effective wake derivation would reproduce the nominal result which would be independent of time and blade position.

The first effective wake harmonic amplitude distribution produces a more nearly constant distribution near the suction side of the blade; the second distribution is more nearly constant near the pressure side of the blade. The difference between the two distributions is the magnitude of the assumed wake amplitude used in the lifting surface calculation. If a further reduced wake distribution were to be used, then a relatively constant harmonic amplitude

would probably result near the pressure side of the blade, and the variation would be greater near the suction side of the blade.

Comparison can also be made between the derived effective wake harmonic amplitudes and the nominal wake amplitudes measured with the LDV and the Pitot tube. The comparison had to be made only for the single cycle of the sixth harmonic wake. The nominal wake measured using the LDV at the propeller plane was harmonically analyzed, using the same estimating assumptions for the missing measurements at the extremities of the wake as were made before, resulting in an amplitude of 0.153. The Pitot tube nominal value was recalculated for the single cycle using the 15 harmonic representation shown in Table 2, which resulted in a value of 0.172. This result was then corrected for the wake decay effect by $C(r)_n$, the multiplicative factor discussed earlier, resulting in an amplitude of 0.151. These values are reasonably close and are shown in Fig. 22 for comparison to the effective results. The nominal results are approximately 12% higher than the effective wake result at the null point. Any further iterations of the propeller-induced velocities would change the effective wake blade-to-blade distribution, but the correlation at the null point would not change.

Therefore in a global sense, effects appear to exist that reduce the nominal wake at the propeller plane, but the blade thrust and torque are generated on the blade surface, so that effective wake velocity should be considered near the blades. In the region near the blades the propeller flow modeling will influence the derived effective wake harmonic. The present model used, PUF-2, appears to be inconsistent in accounting for the induced velocities on the suction and pressure sides of the blade, probably because of insufficient representation of blade thickness effects in the lifting surface model.

DISCUSSION

This report describes further understanding of unsteady propeller hydrodynamics as it relates to the prediction of unsteady propeller shaft loads. Measurements of unsteady thrust and torque were obtained for two propellers operating in various screen-generated simple axial harmonic wakes. Velocity measurements were obtained at the propeller centerline for a given wake to investigate the effect of the propeller on the incoming flow. The velocity fields and the loads were predicted using unsteady lifting surface theory. The primary issue in this work was the accuracy of current unsteady force prediction codes.

BLADE VIBRATION ASSOCIATED WITH 12 CYCLE WAKE SCREEN

Figure 16 shows the final comparison of the measured and predicted unsteady thrusts and torques for the various wake screen configurations used. Phase comparisons are presented in Fig. 12. A significant trend in the correlation is the underprediction occurring the 12th harmonic screen. This trend is possibly due to resonant blade vibration excited by the 12th harmonic wake.

The effect of blade vibration on unsteady force response was studied by Brooks⁹ in great detail using the same dynamometry as the experiments described in this report. Brooks measured unsteady thrust and torque on two seven-bladed propellers operating behind a seven-cycle wake screen. Measurements were made at constant advance coefficient over a wide range of

propeller rotation speeds. Measured load response was found to be amplified about the resonant frequency associated with cantilever mode blade vibration. The amount of amplification was attributed to the amplitude of the hydrodynamic damping coefficient. Low damping was associated with the wide-bladed propeller and high damping was associated with the narrow-bladed propeller.

After the tests reported here, concern about the effect of blade vibration led to a check of the blade resonant frequencies of the propellers tested. The propeller was mounted on the dynamometer submerged in water. The blades were tapped normal to the blade surface and the thrust and torque responses were monitored on a storage oscilloscope. This crude technique was used to measure the approximate blade resonance frequency for Propeller 4119. The resonant frequency of Propeller 4119 was found to be 185 Hz. Propeller 4132 was not available for checking its resonance characteristics, but it was probably similar to Propeller 4119. The excitation frequency for the 12th harmonic screen case was 120 Hz, so it is believed that some force amplification did occur for the 12th harmonic screen configuration.

Quantitative corrections to the existing data for this effect would not be appropriate because measurements over a range of speeds are lacking. The present correlations of measured and predicted results in Fig. 16 support a blade vibration effect. Generally both propellers show an underprediction for the 12th harmonic screen results, with a more extreme underprediction for Propeller 4119, perhaps due to less hydrodynamic damping with the wider-bladed Propeller 4119 or a higher resonant frequency associated with Propeller 4132. The observed correlation and the previous work of Brooks⁹ indicate that the underprediction for the 12th harmonic data is due to blade resonance.

THE ROLE OF EFFECTIVE WAKE IN UNSTEADY FORCE PREDICTIONS

The overall goal of the effective wake study was to improve the prediction of unsteady propeller forces. Effective wake calculations for flow between the blades show that the propeller tended to reduce the nominal wake harmonic amplitude by 12%. The correlation shown in Fig. 16 between measured and predicted forces for this case, Propeller 4132 in the 6th harmonic wake, is very good, presenting a dilemma, since a reduction in the nominal wake by 12% will then result in an underprediction of the measured unsteady forces. An implication from this result is that other effects have not been captured in the modeling of the unsteady hydrodynamics. The usefulness of the effective wake result is limited to the observation that the propeller has some effect on the incoming wake harmonic structure.

CONCLUSIONS AND RECOMMENDATIONS

Systematic wake and unsteady force measurements were conducted on model propellers operating in idealized screen-generated axial wakes. A Laser Doppler Velocimetry system was used to measure near field velocities while the propeller was operating to assess the influence of the propeller on the nominal inflow wake. The following conclusions have been made:

1. The experience of measuring both the inflow wake and the forces showed the two quantities to be equally elusive. Accurate measurements of the exciting wake and of the propeller's influence on the wake are important if improvements in prediction accuracy are to be made.

2. Decay of inflow wake amplitude streamwise through the propeller may influence unsteady propeller forces on the order of 5%.

3. The nominal inflow wake harmonics may be altered by 10% by the operation of the propeller in the wake field.

4. For unsteady propeller shaft forces occurring at one through four times blade rate frequencies, PUF-2 predictions of thrust and torque amplitudes are accurate to within 25%; predictions of phase are accurate to within 20 degrees.

5. Prediction of unsteady forces appears to be more accurate with the narrower-bladed propeller (EAR=0.3) than with the wider-bladed propeller (EAR=0.6).

It is recommended that further experiments be conducted to obtain more accurate measurements of the wake through the propulsor. Also tests conducted over a range of speeds would permit characterization of the dynamic response of the blade, allowing correction of the measured forces to those of the rigid blade assumed in the prediction methods. Such work would increase the overall measurement accuracy and permit further refinement in prediction methods.

ACKNOWLEDGMENTS

The author gratefully acknowledges the assistance of James Fagan and Glen Coty in conducting the test and preliminary data reduction and of Don Fuhs in running and understanding the unsteady lifting surface theory code. Rich Corpus did the initial debugging and running of the field point velocity calculation from the unsteady lifting surface theory.

RADIUS, %

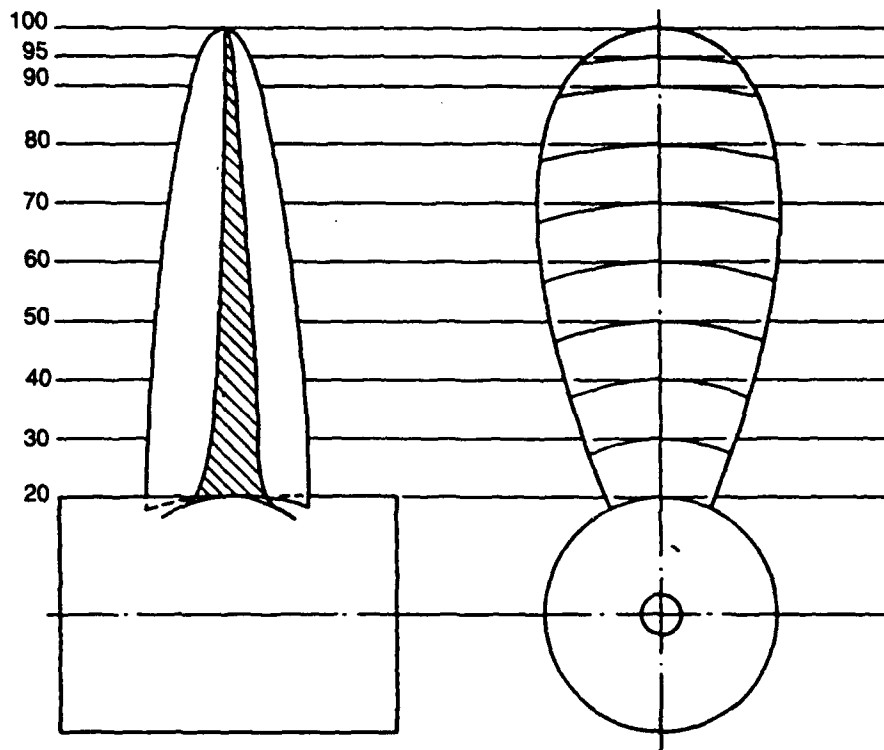


Fig. 1a. Propeller 4132, EAR = 0.3.

RADIUS, %

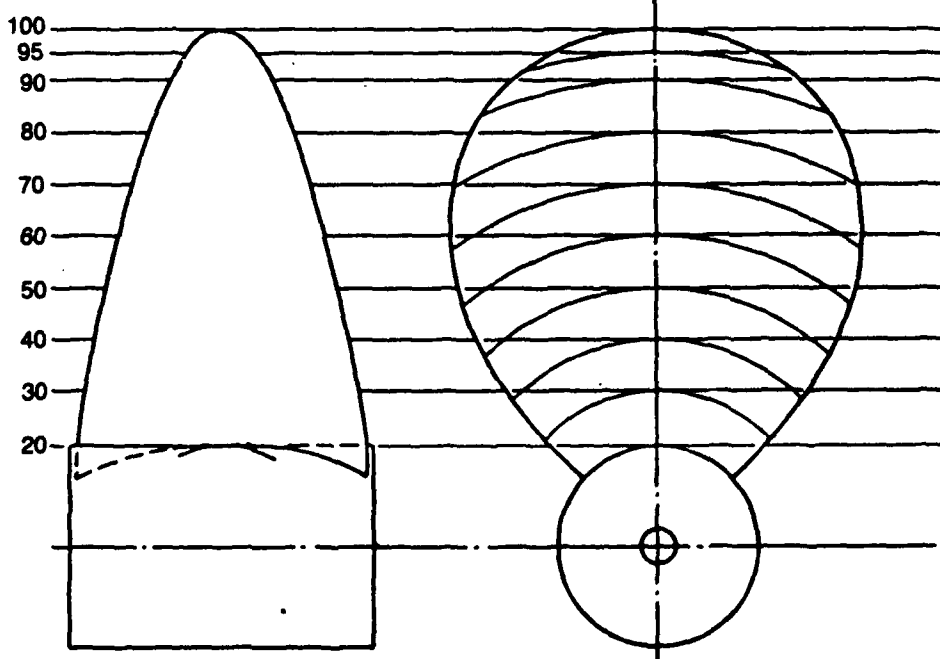


Fig. 1b. Propeller 4119, EAR = 0.6.

Fig. 1. Propellers tested.

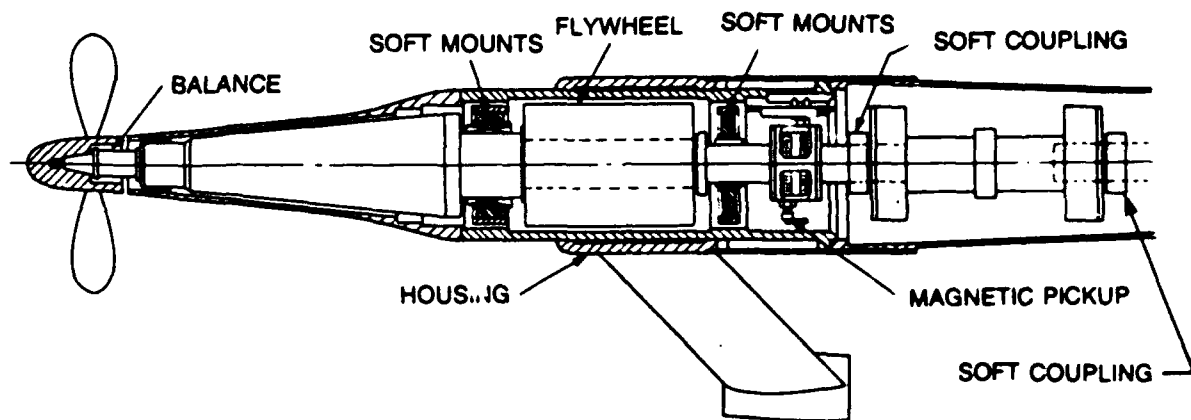


Fig. 2. Six-component propeller dynamometer assembly.

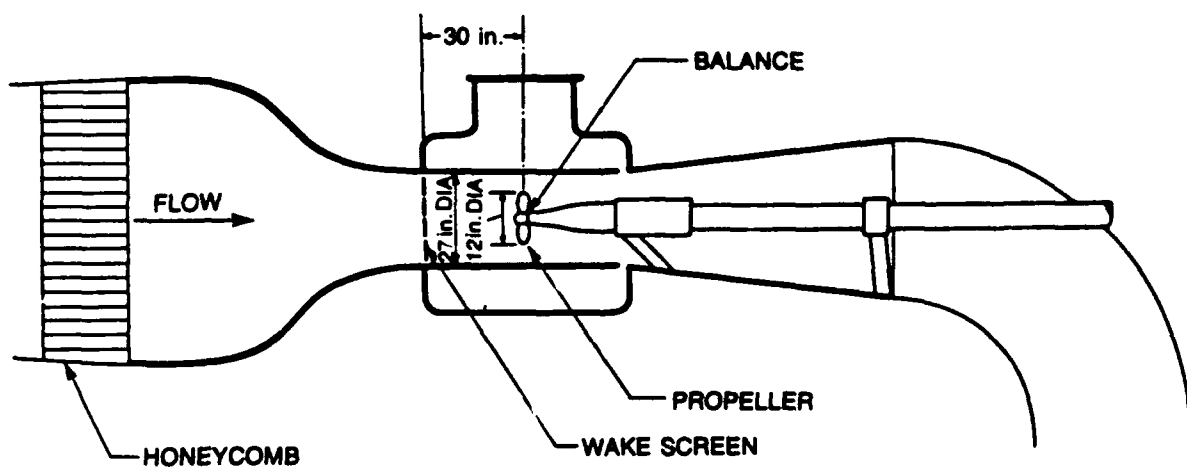


Fig. 3. Test setup.

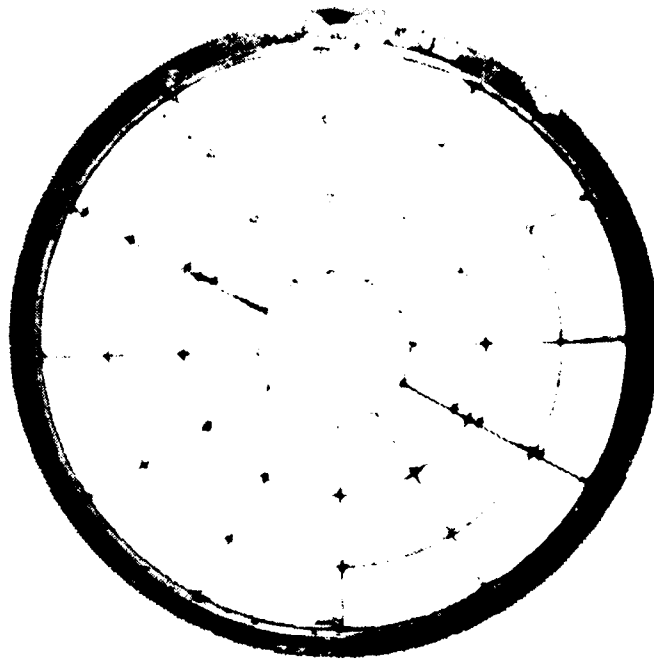


Fig. 4. Wake screen support.

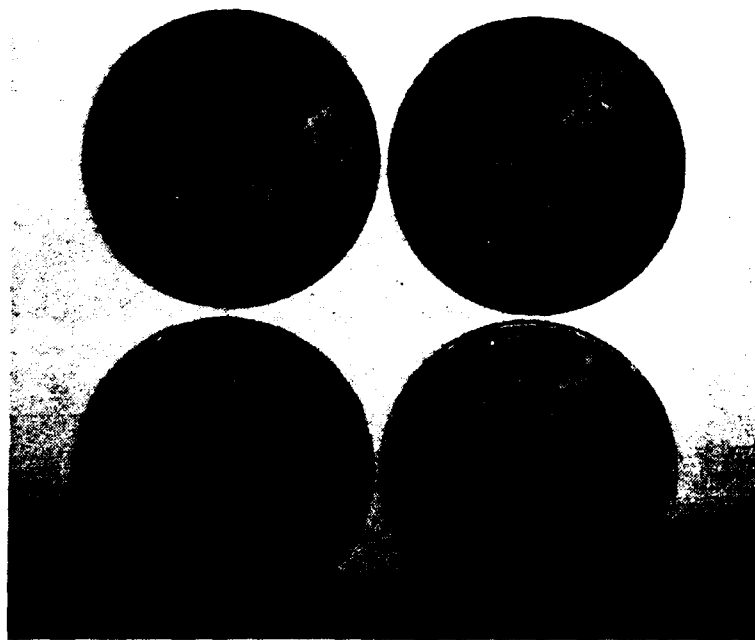


Fig. 5. Wake screens.

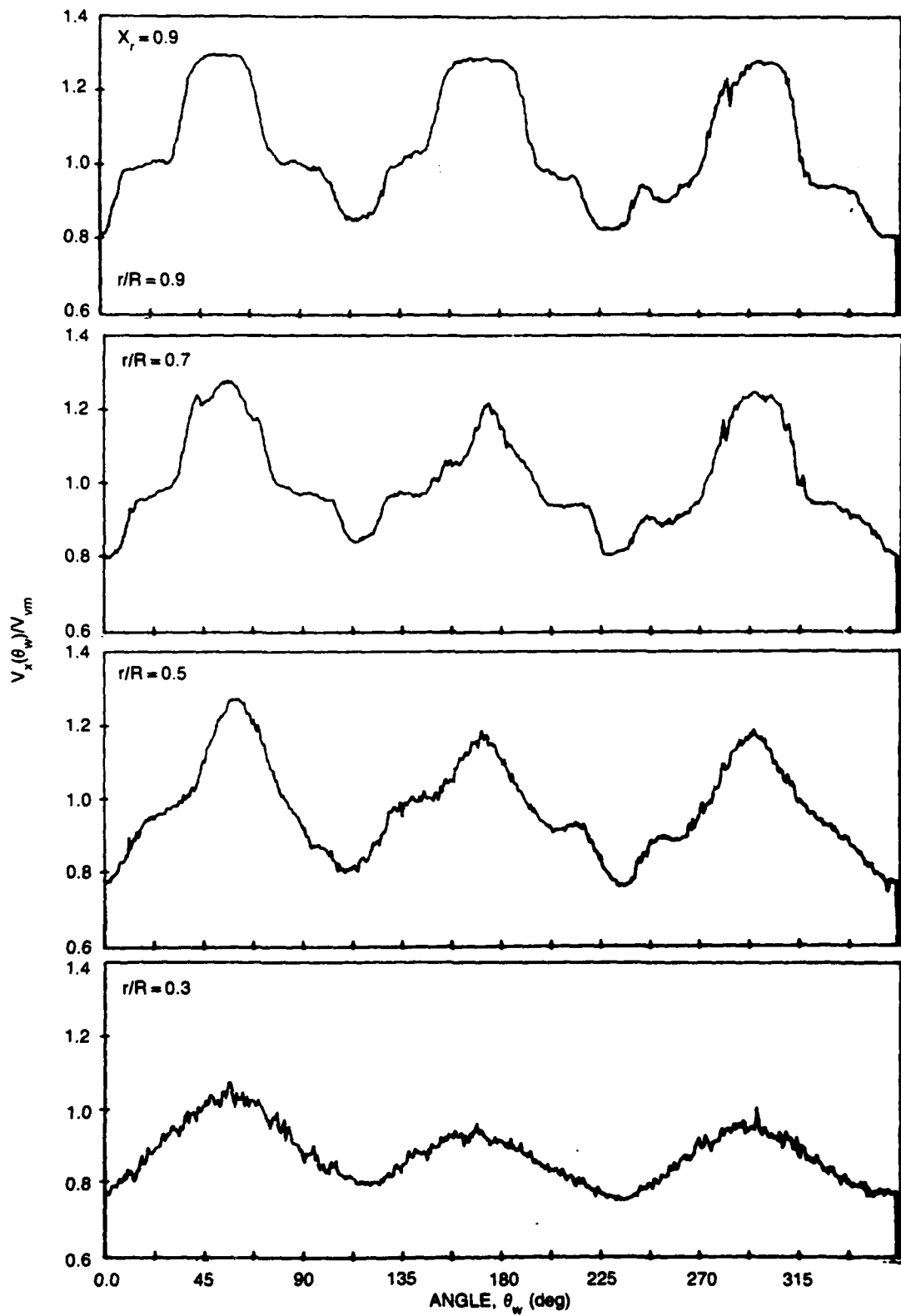


Fig. 6a. Three-cycle wake screen.
 Fig. 6. Measured nominal wakes generated by screens.

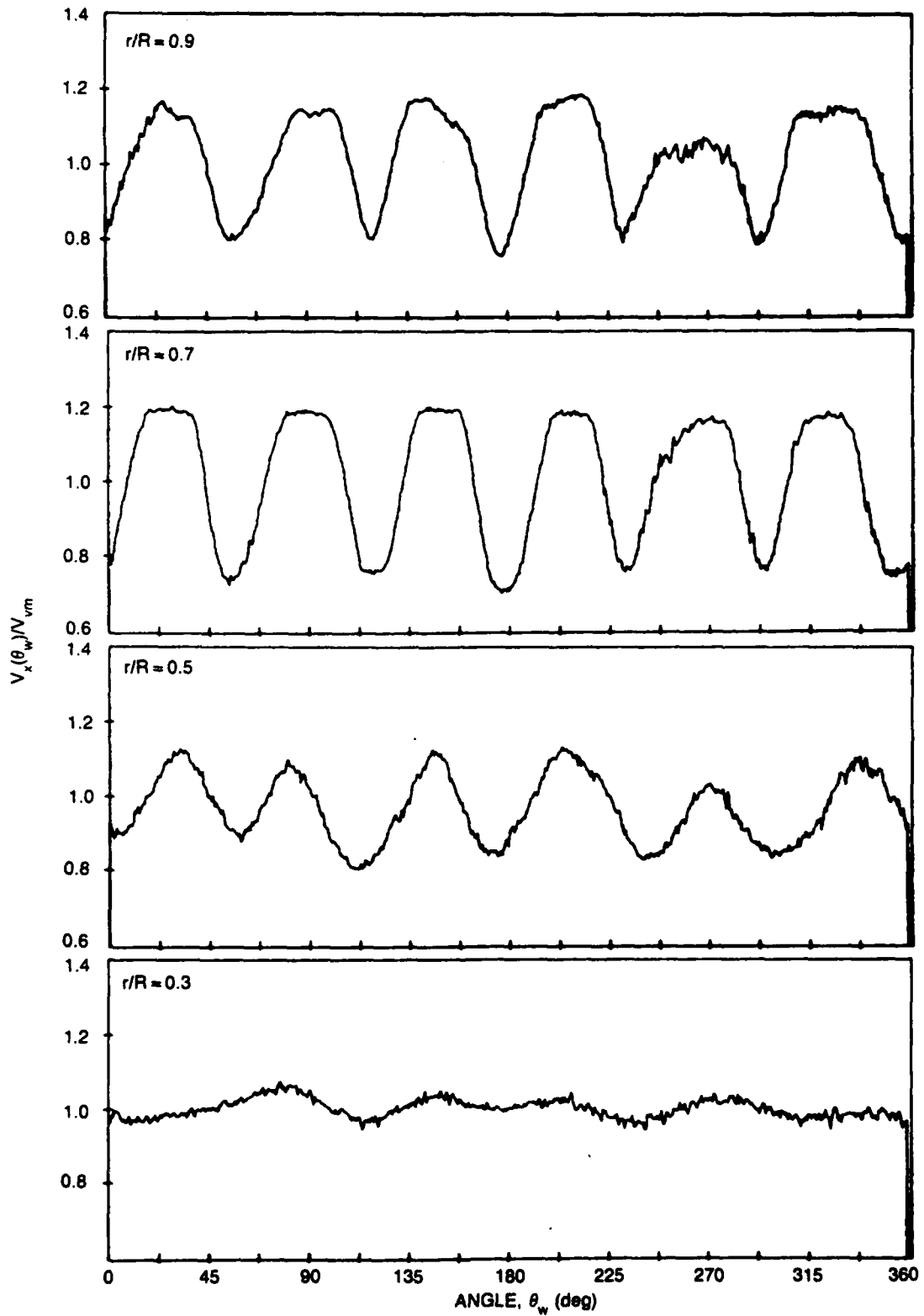


Fig. 6b. Six-cycle wake screen.

Fig. 6. (Continued)

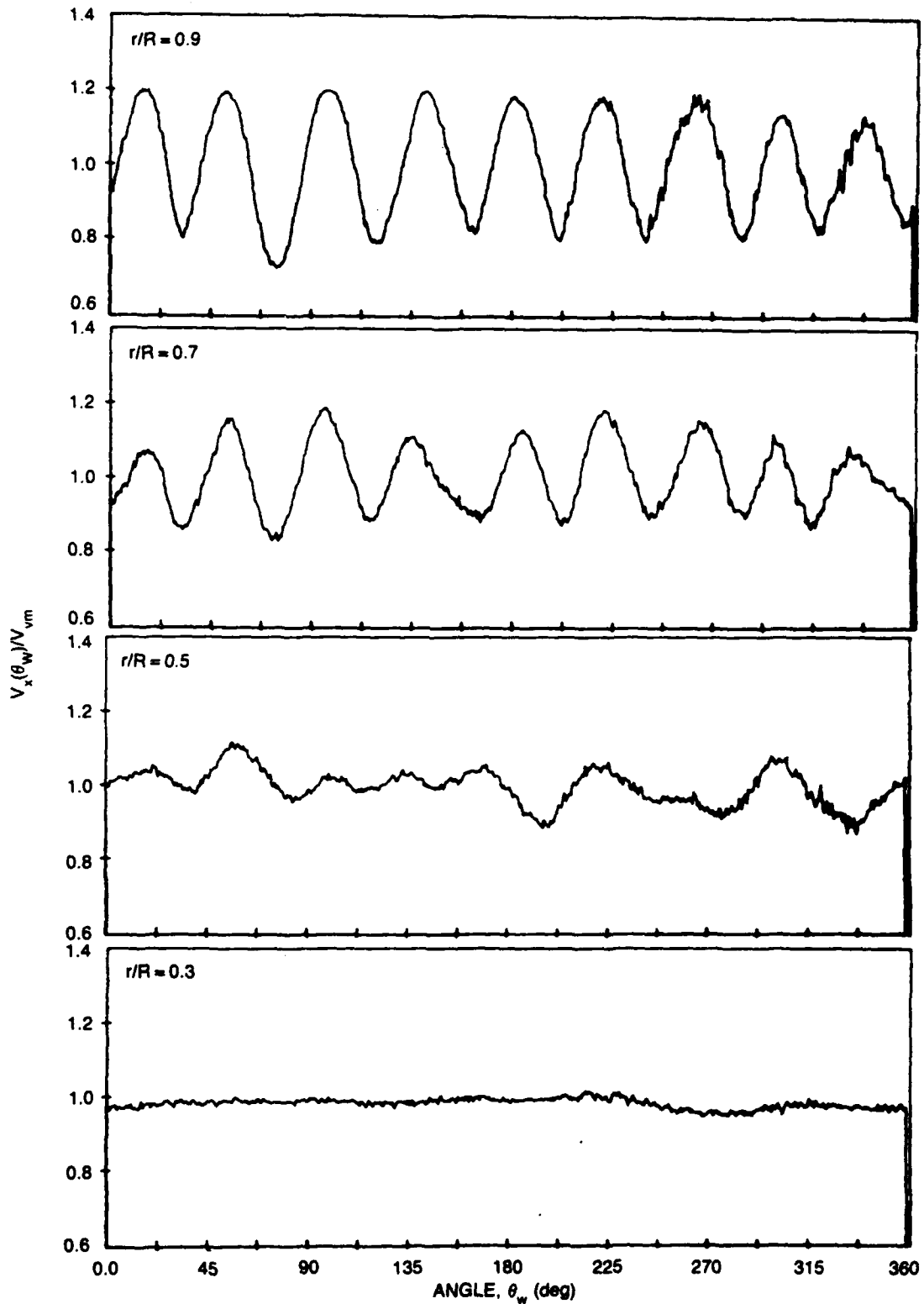


Fig. 6c. Nine-cycle wake screen.

Fig. 6. (Continued)

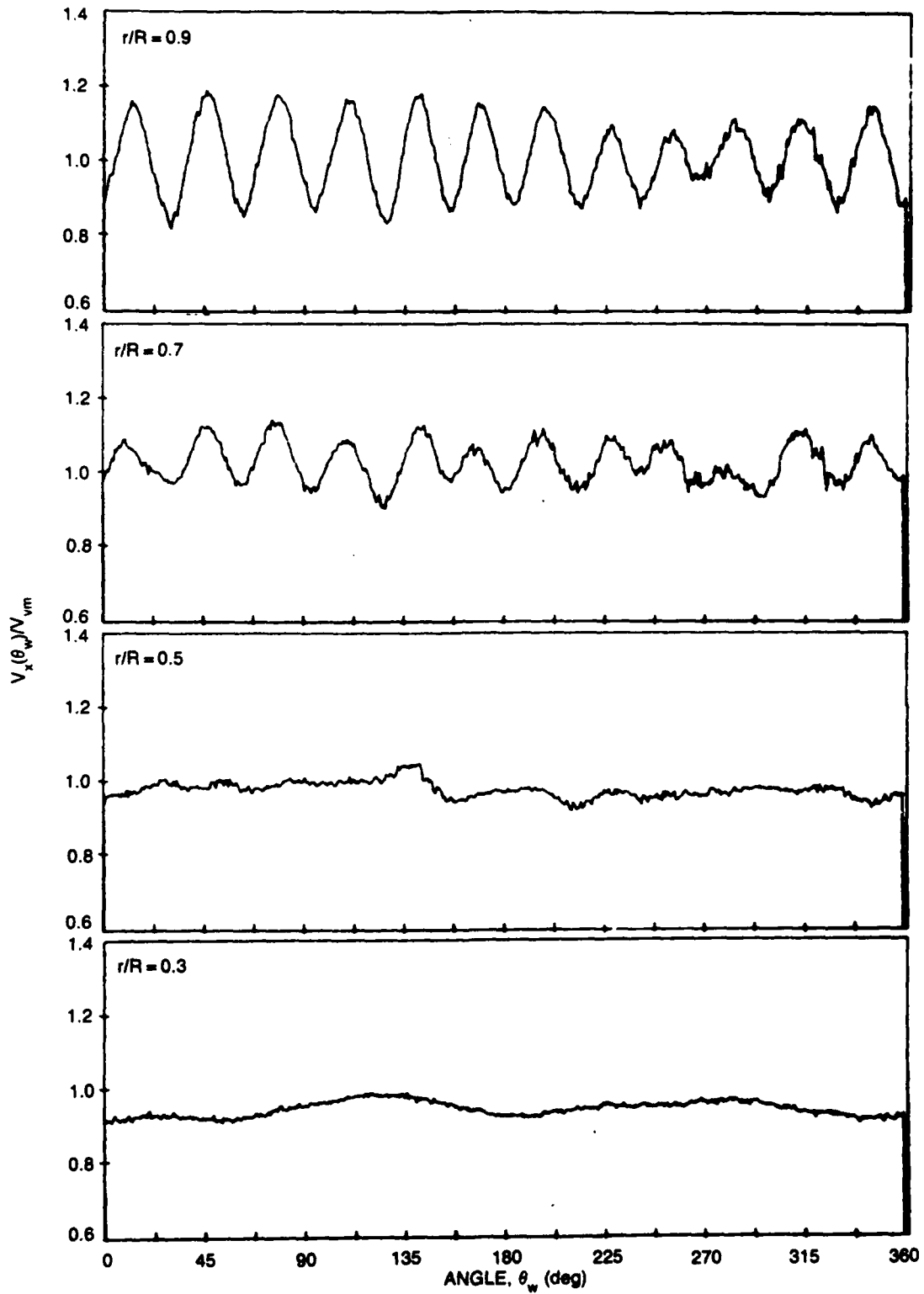


Fig. 6d. Twelve-cycle wake screen.

Fig. 6. (Continued)

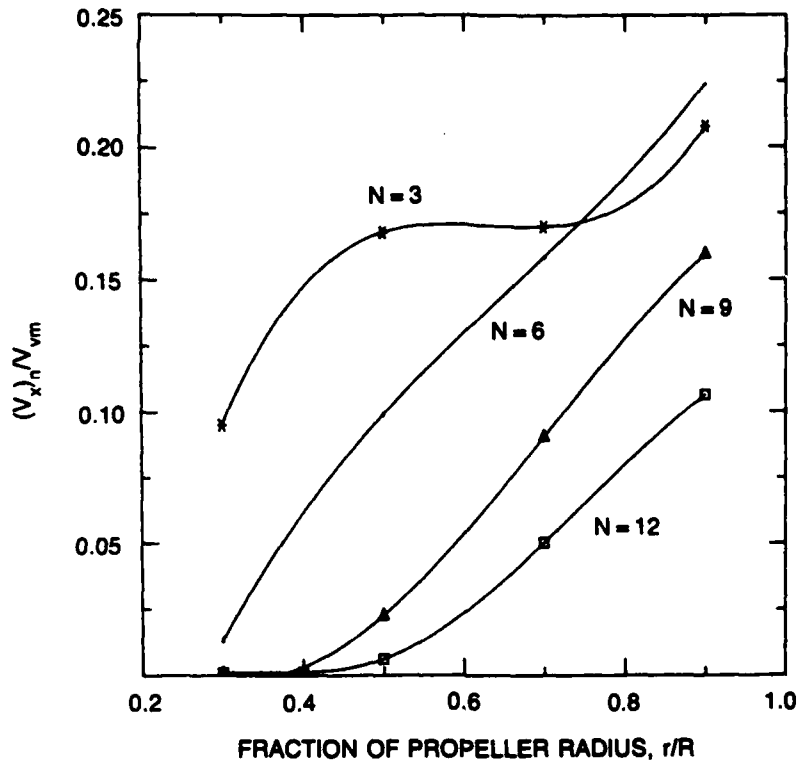


Fig. 7. Nominal wake harmonic amplitudes generated by screens.

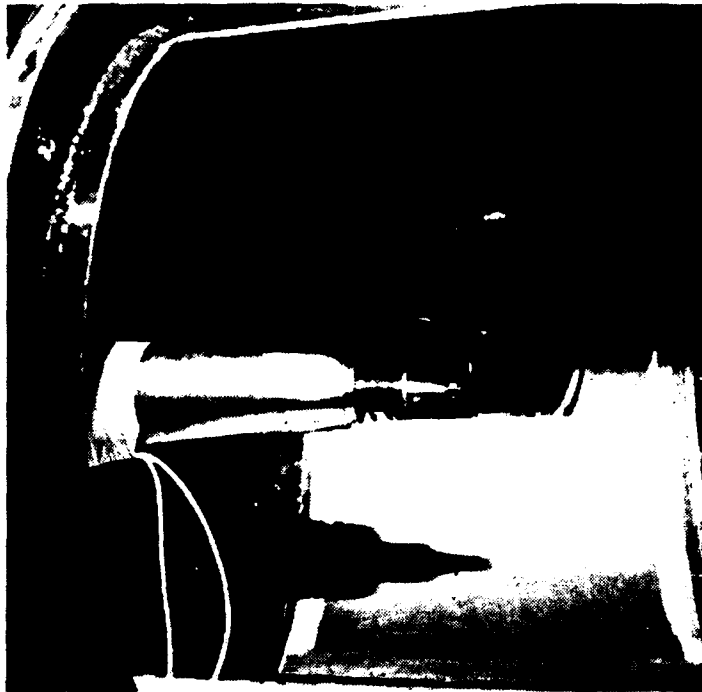


Fig. 8. Test setup showing a dynamometer, closed jet test section, and tunnel window insert.

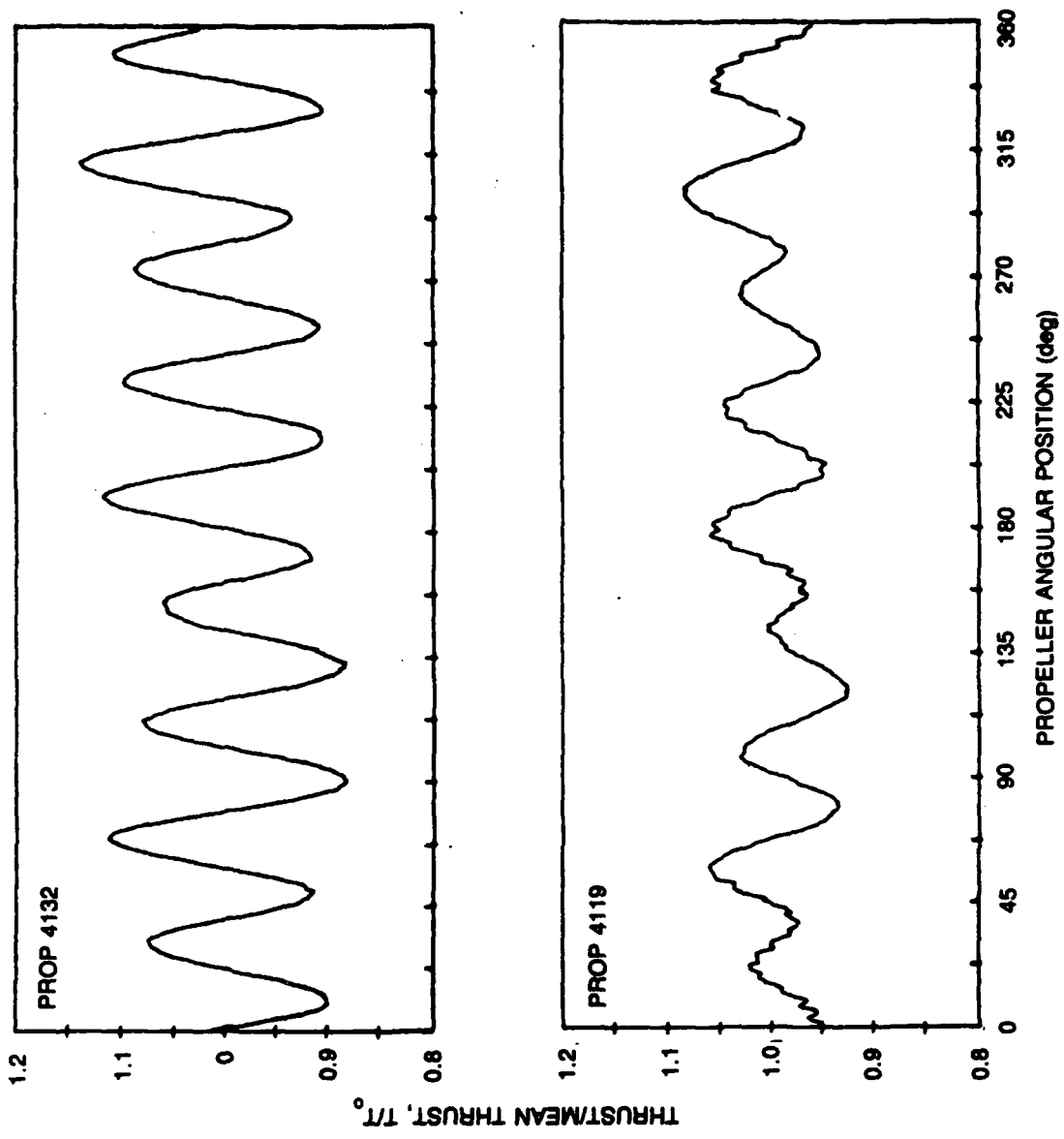
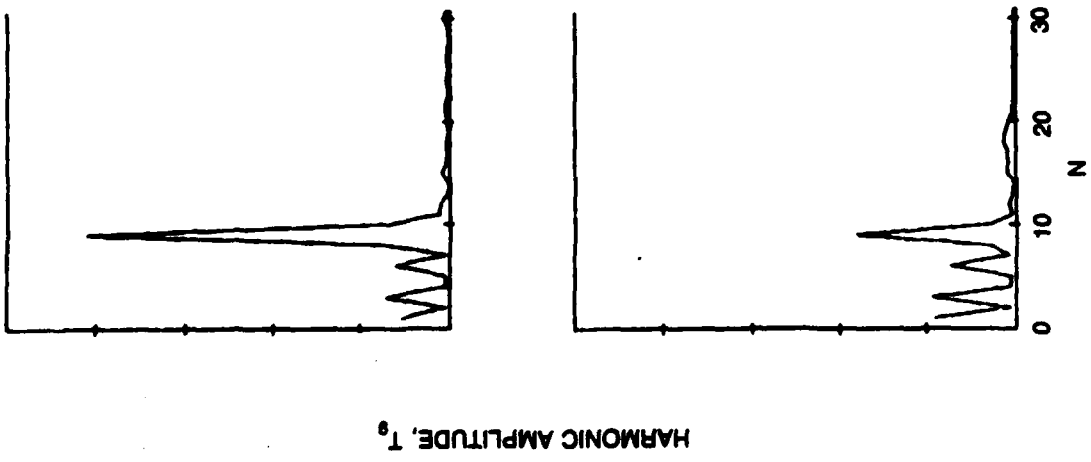


Fig. 9a. Thrust measurements for nine-cycle screen.

Fig. 9. Unsteady thrust measurements.

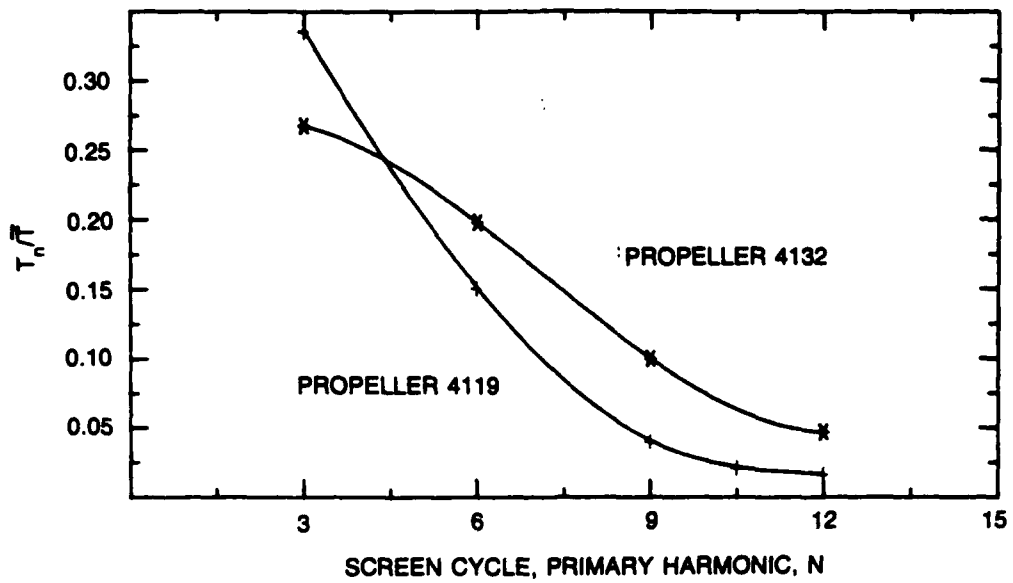


Fig. 9b. Harmonic thrust amplitude for wake screens tested.

Fig. 9. (Continued)

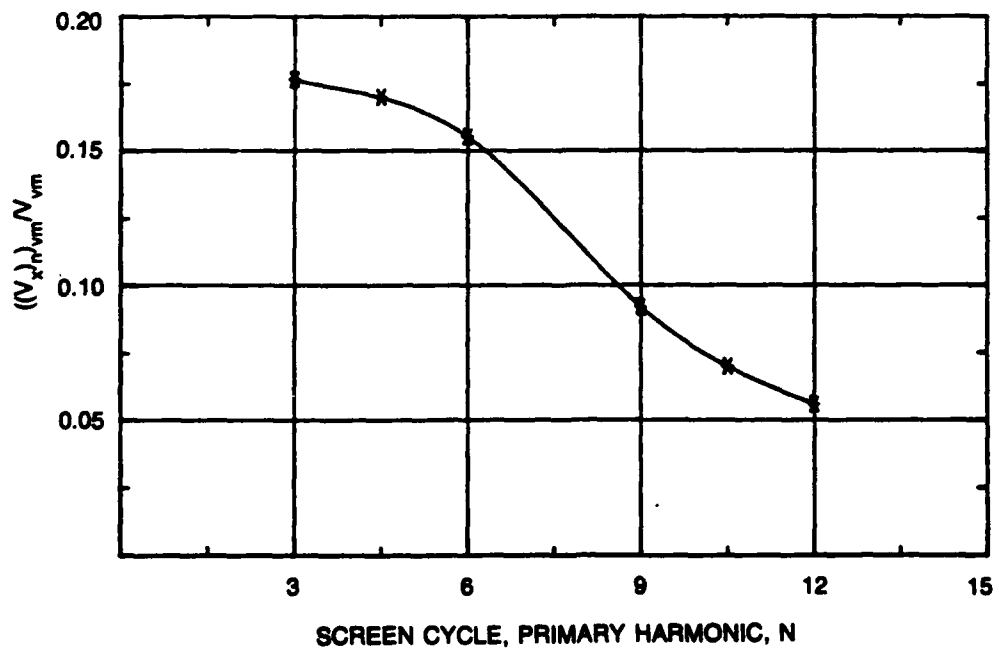


Fig. 10. Volume mean wake harmonic amplitudes for wake screens tested.

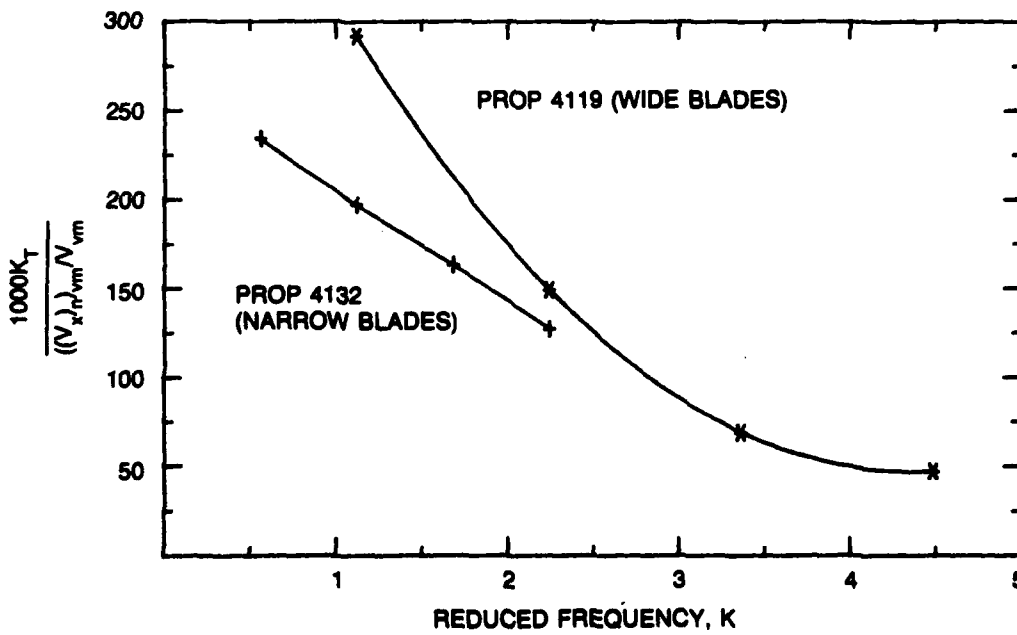
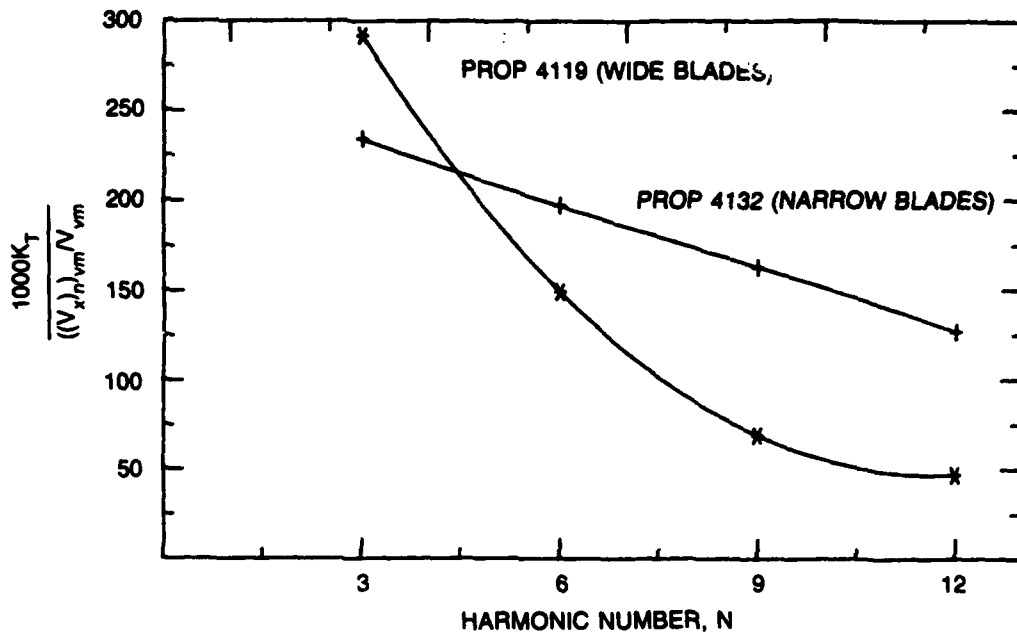


Fig. 11. Variation of unsteady thrust with harmonic number and reduced frequency.

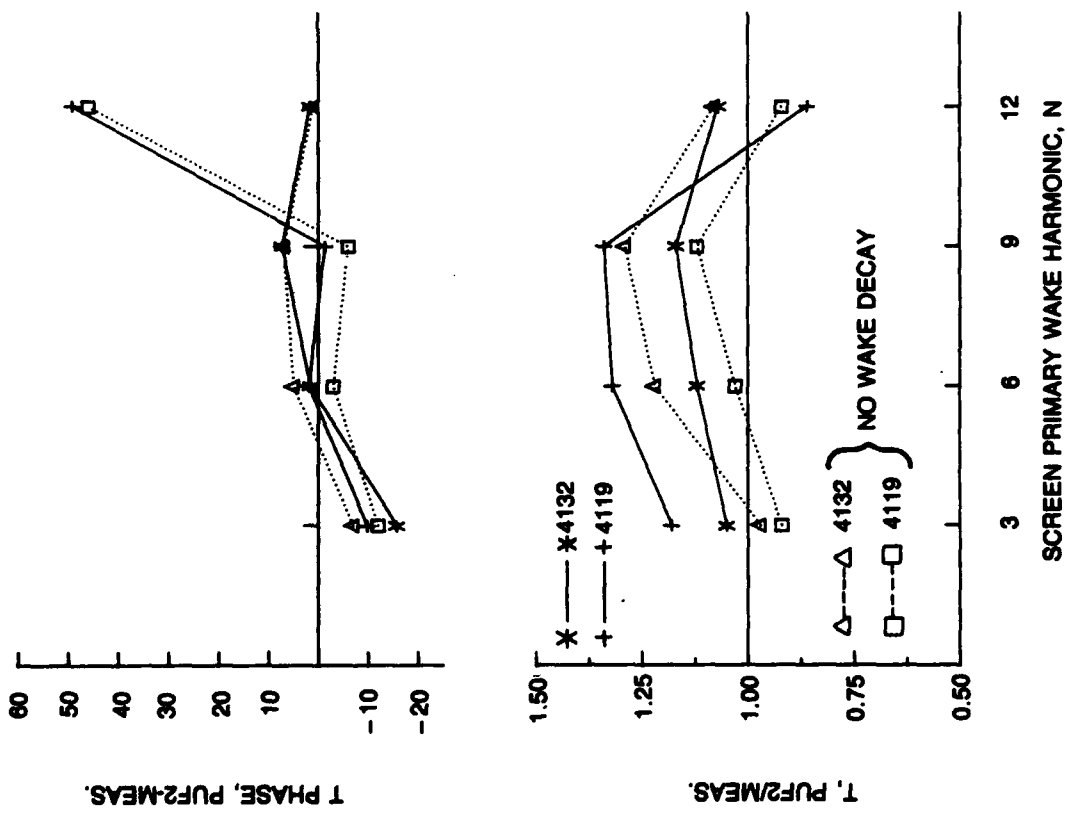
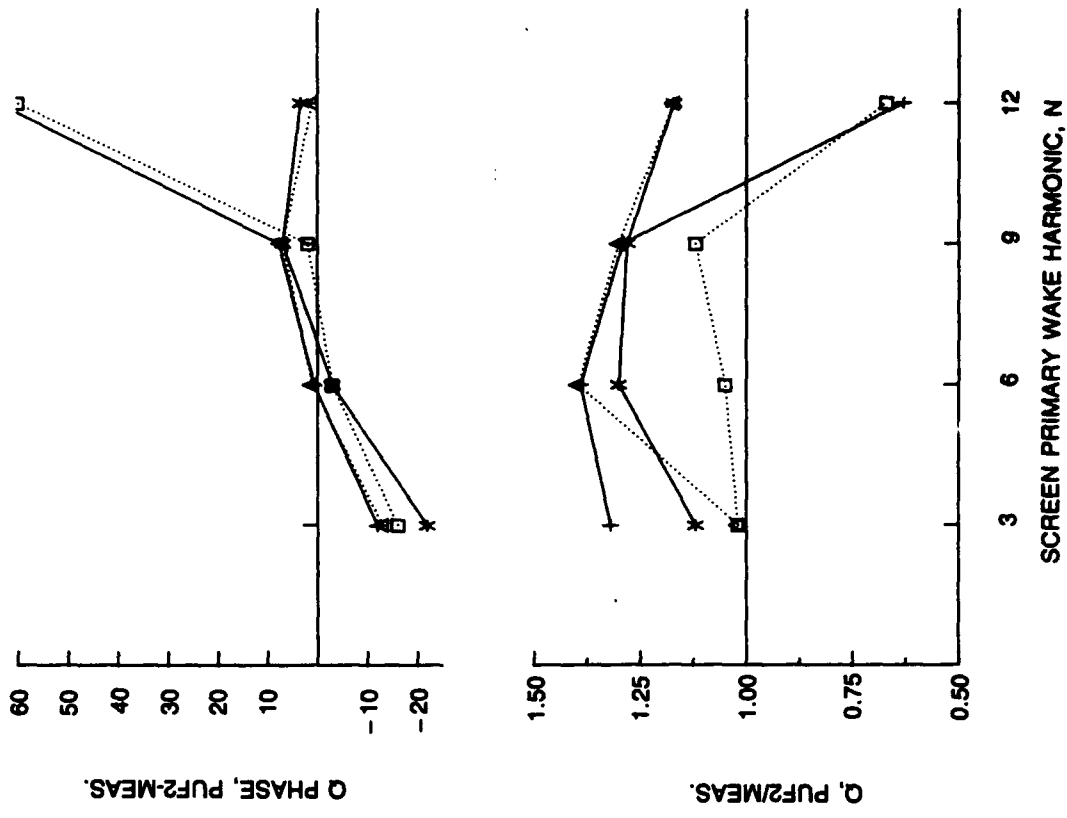


Fig. 12. Comparison of calculated and measured unsteady propeller forces.

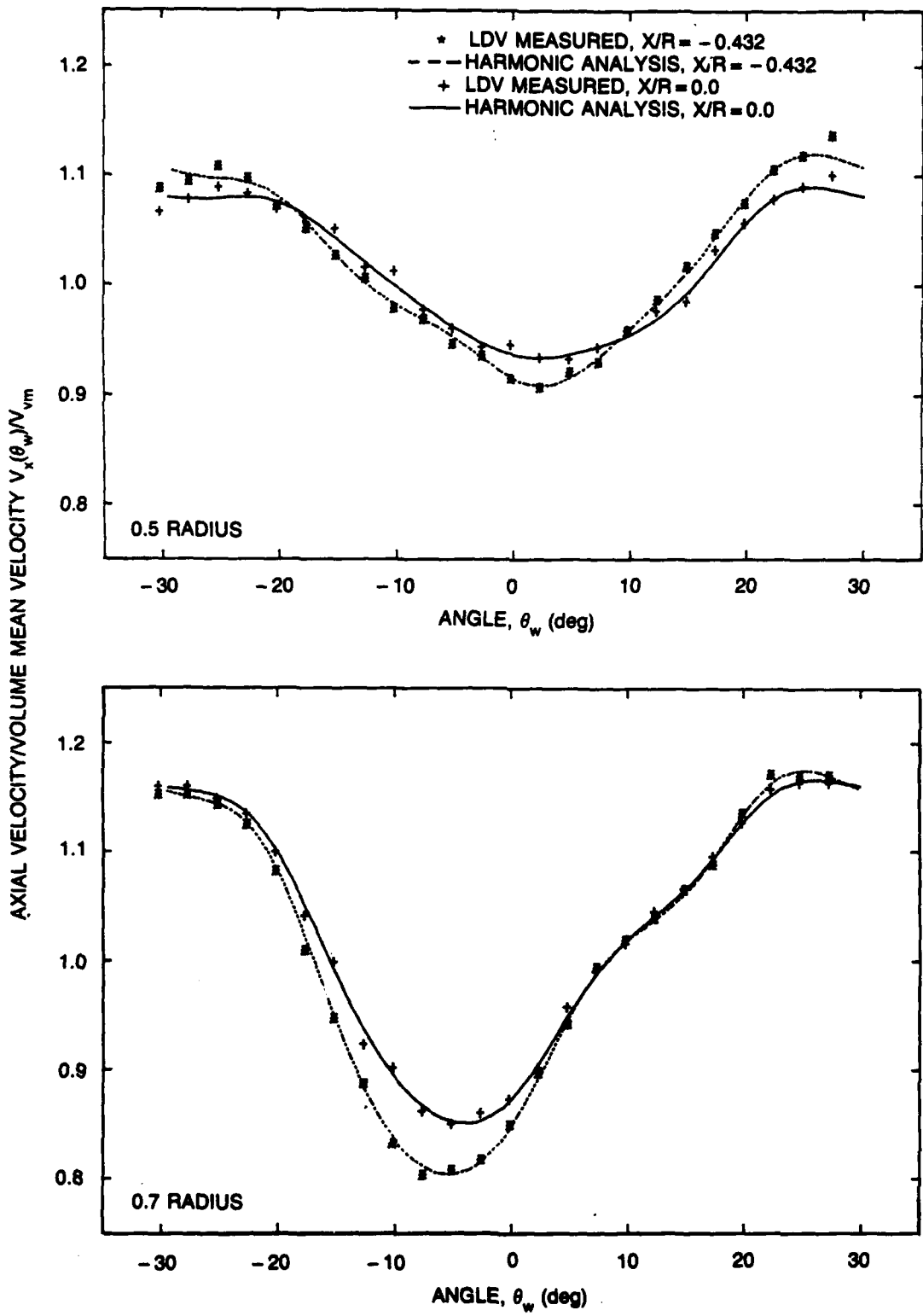


Fig. 13. Decay of six-cycle wake from forward plane to propeller plane.

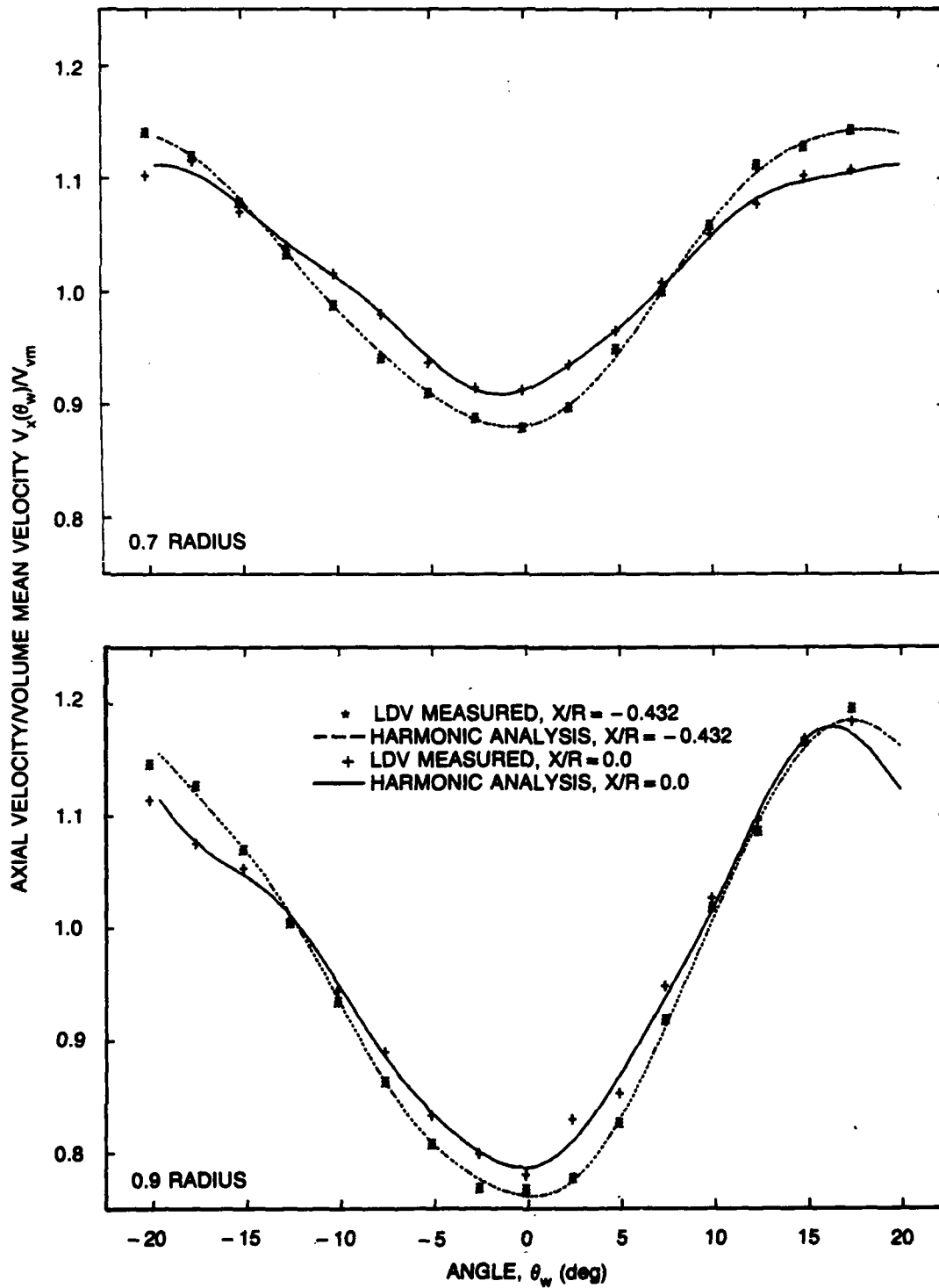


Fig. 14. Decay of nine-cycle wake from plane to propeller plane.

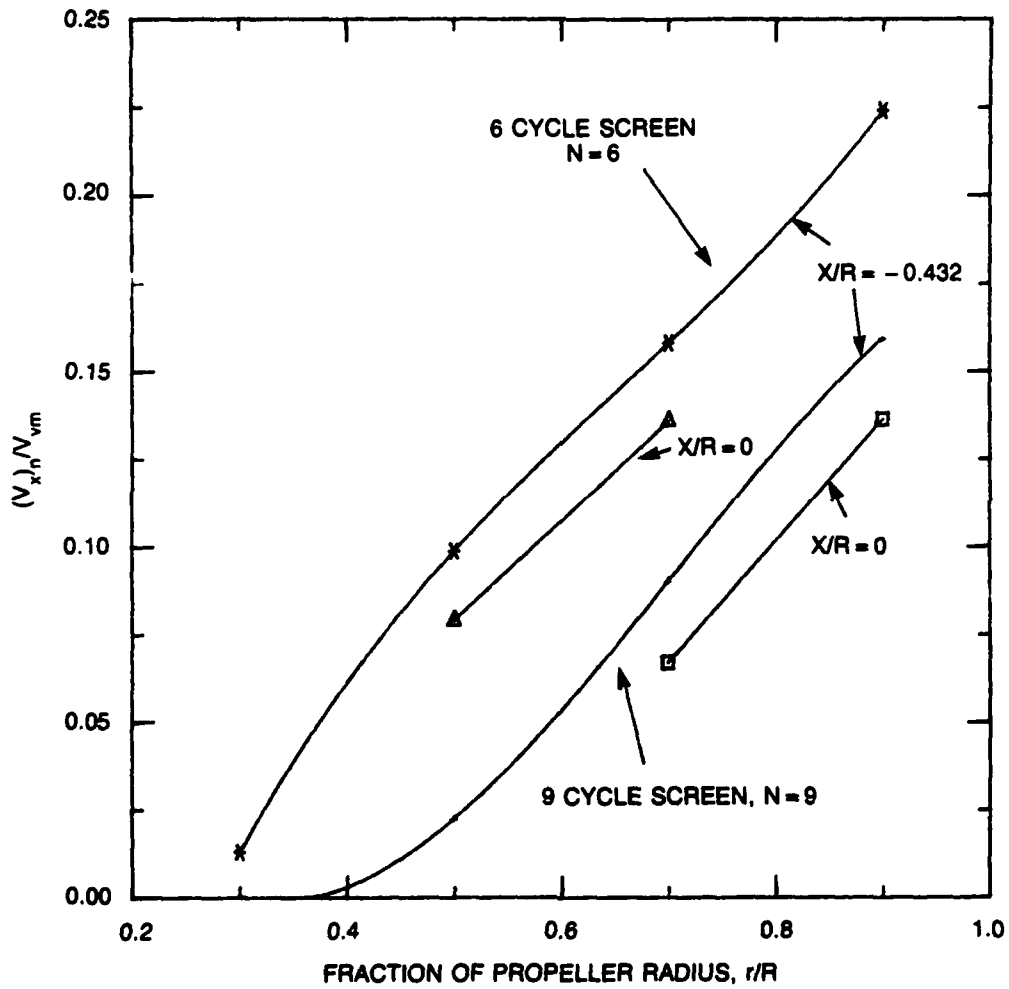
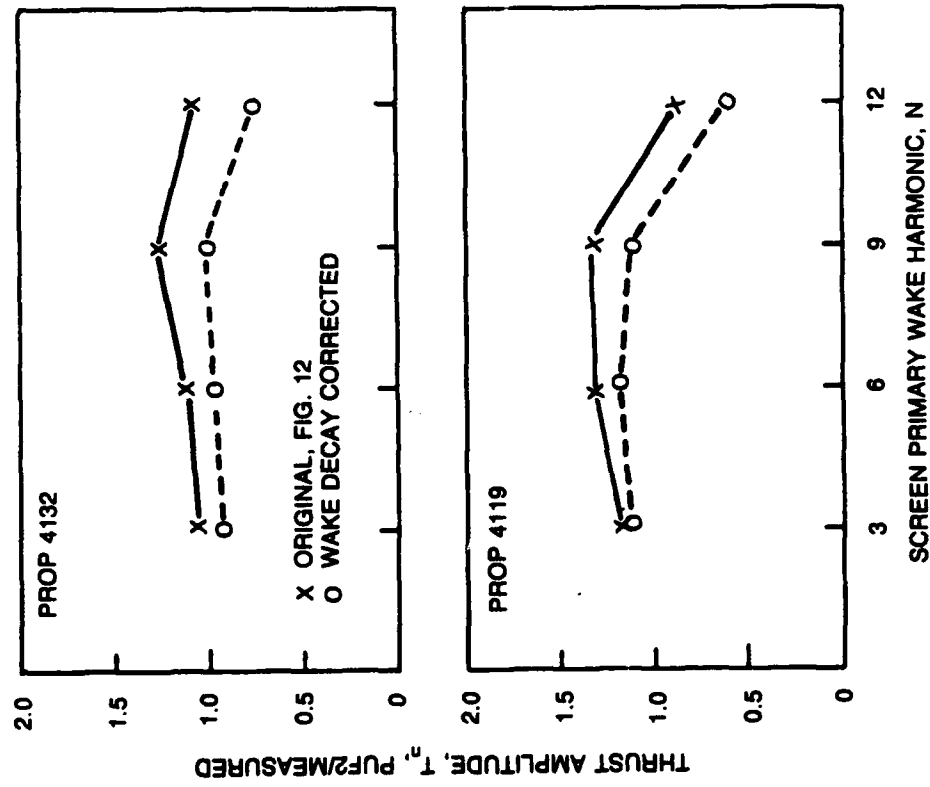
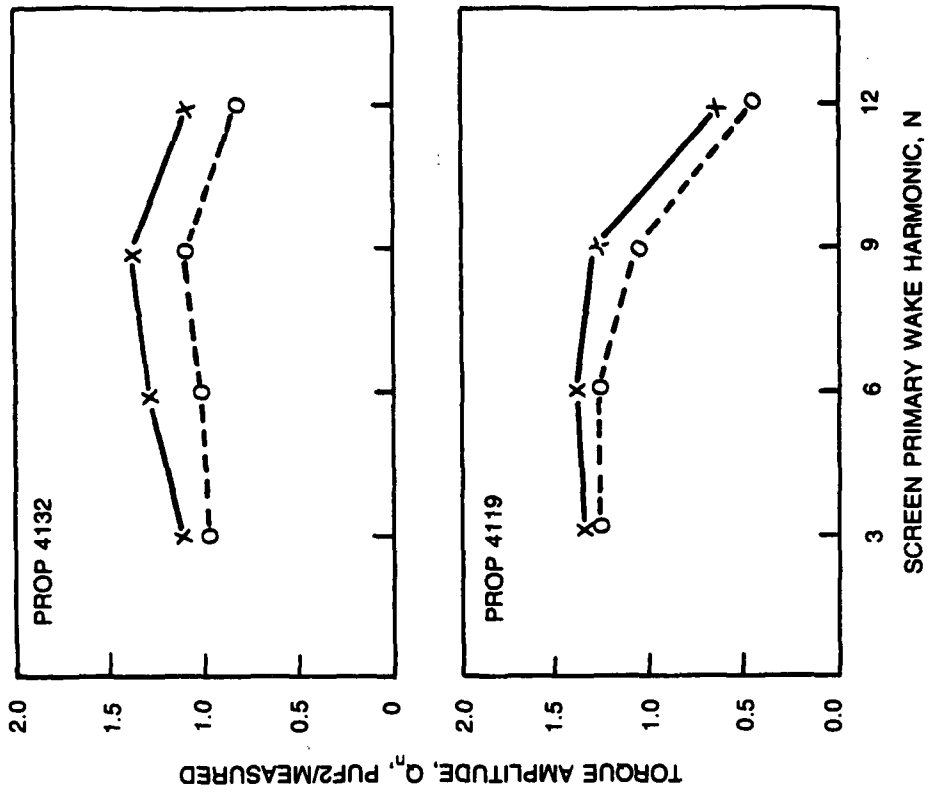


Fig. 15. Reduction of wake harmonic amplitudes due to wake decay from forward pitot tube plane propeller plane.



*WAKE DECAY REPRESENTED BY REDUCING PRIMARY WAKE HARMONICS, $(V_x)_n / V_{vm}$ BY 0.022 UNIFORMLY OVER RADIUS.

Fig. 16. Influence of wake amplitude decay on correlation of measured forces with PUF-2 prediction.*

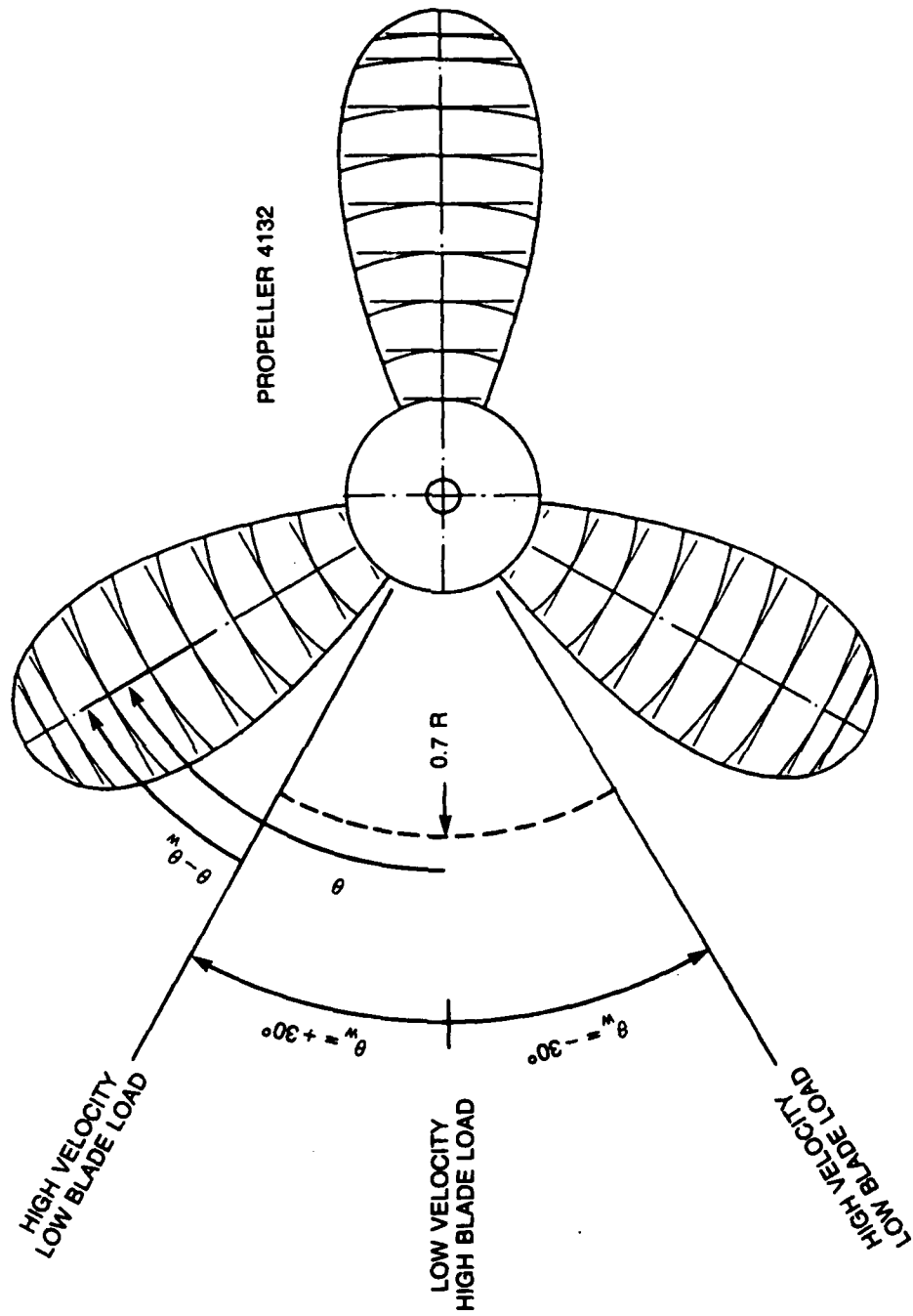


Fig. 17. Total velocity measurement positions using LDV.

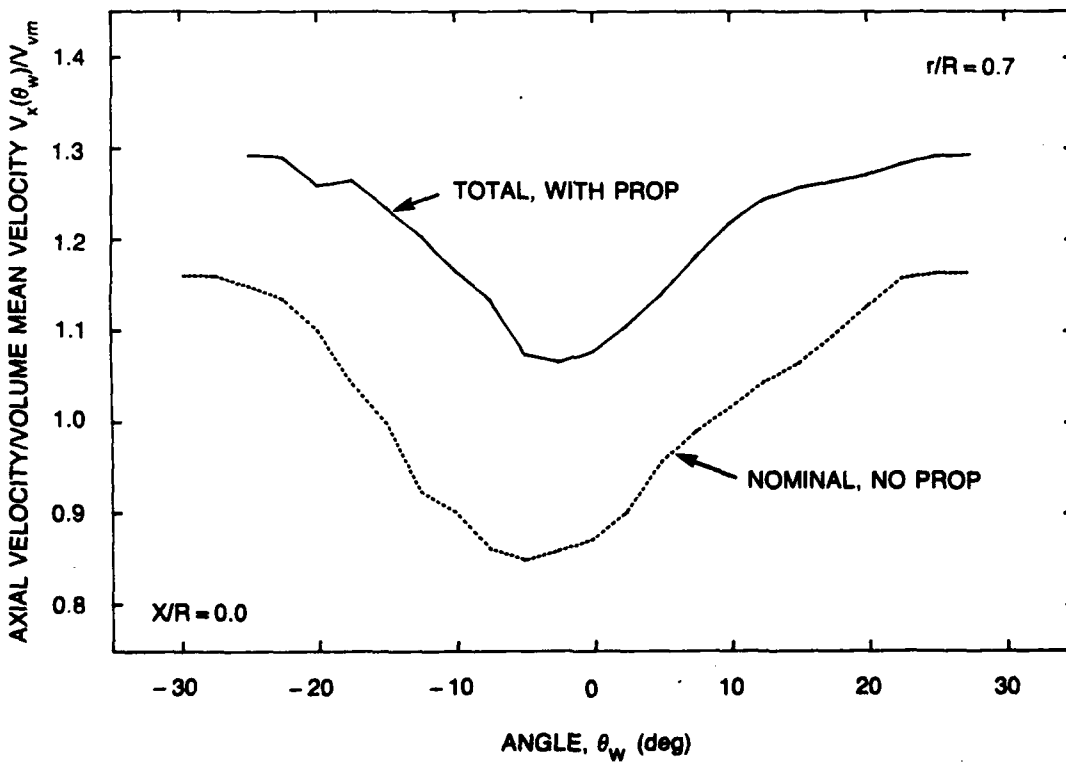
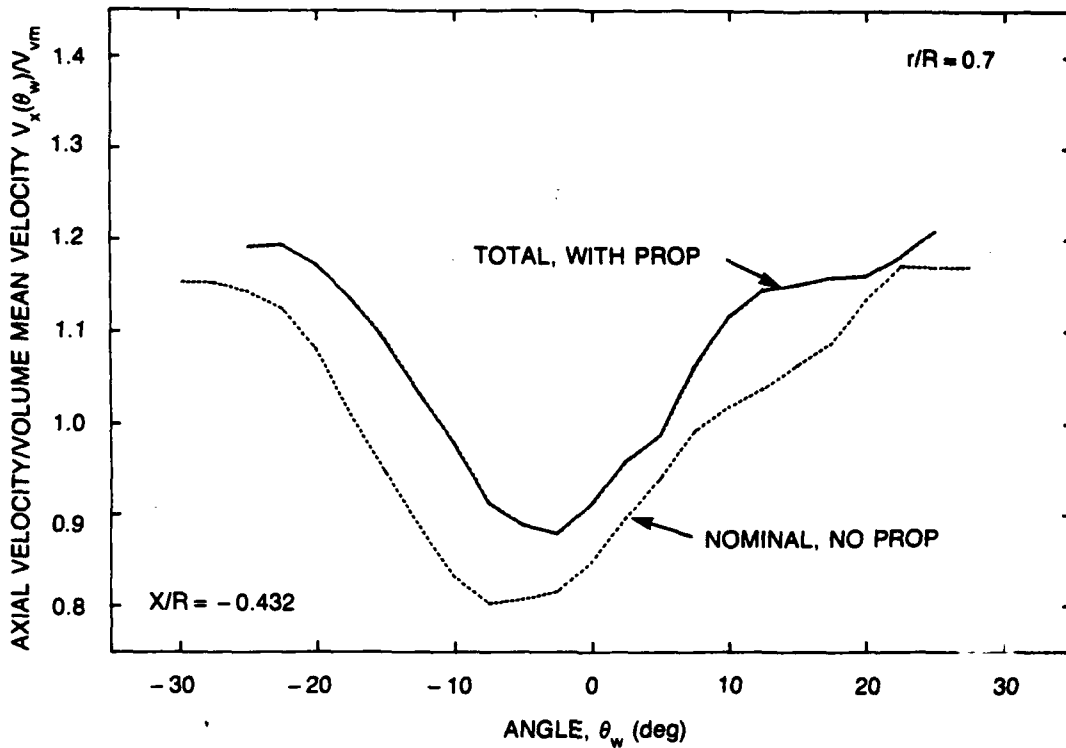


Fig. 18. Comparison of LDV measured time average velocity with and without propeller operating at forward plane and propeller plane.

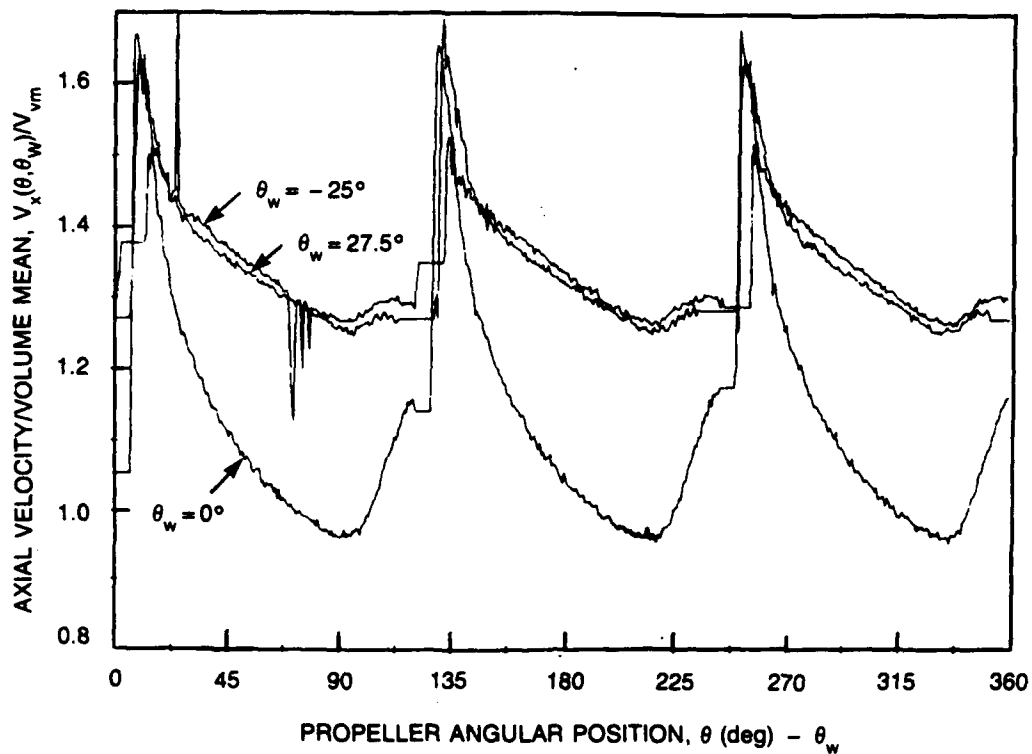


Fig. 19a. Profiles showing complete rotation of propeller.

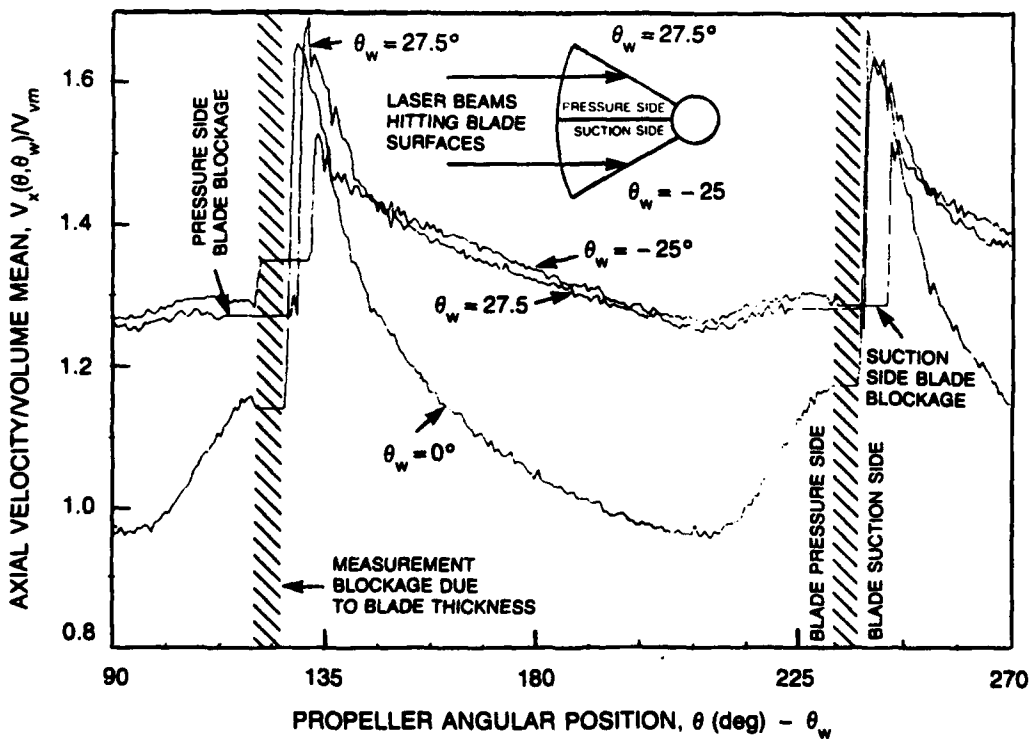


Fig. 19b. Profiles showing one-blade passage.

Fig. 19. Variation of total axial velocity with propeller angular position, measured at propeller axial centerline at three positions in the six-cycle wake.

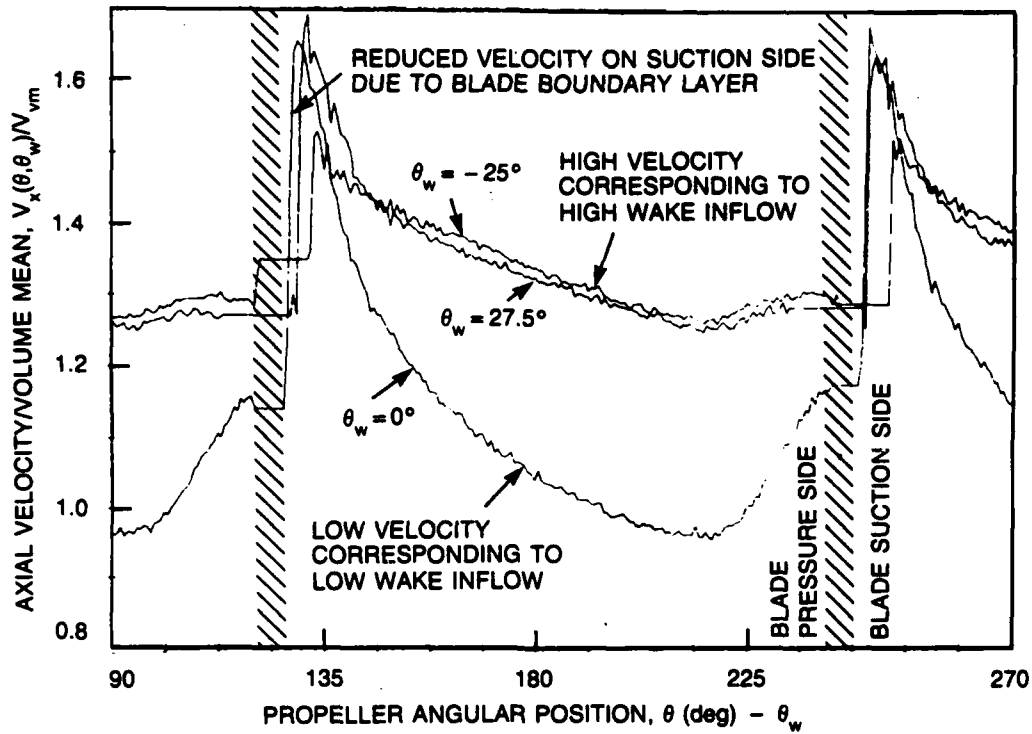


Fig. 19c. Profiles showing one-blade passage.

Fig. 19. (Continued)

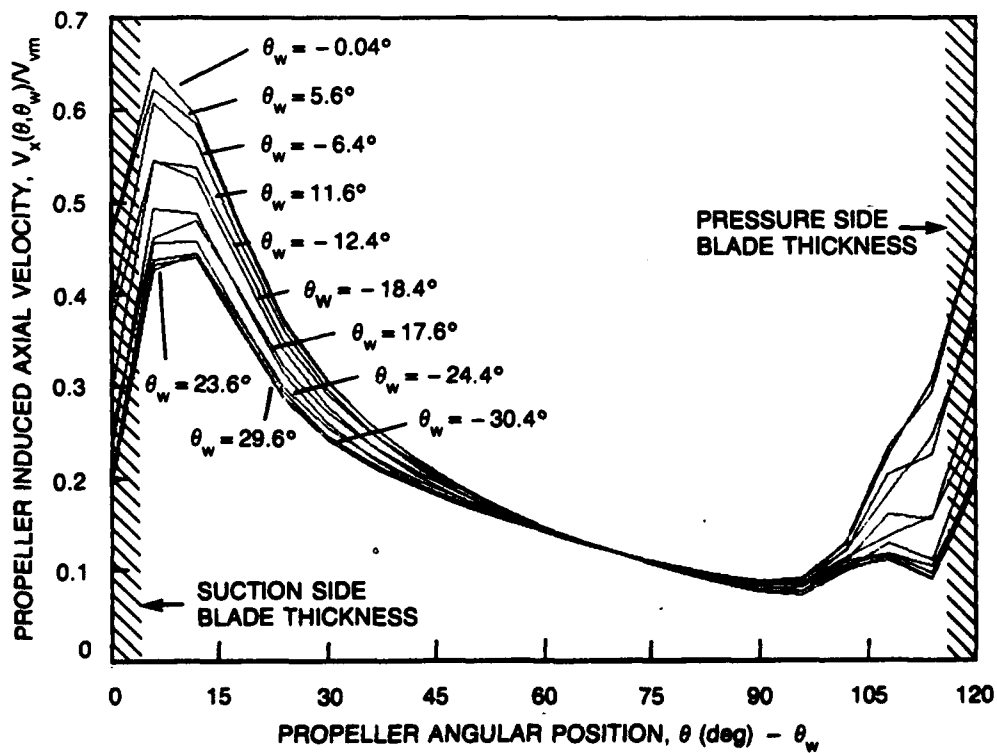


Fig. 20. Variation of blade-to-blade induced velocity at various positions in six-cycle wake.

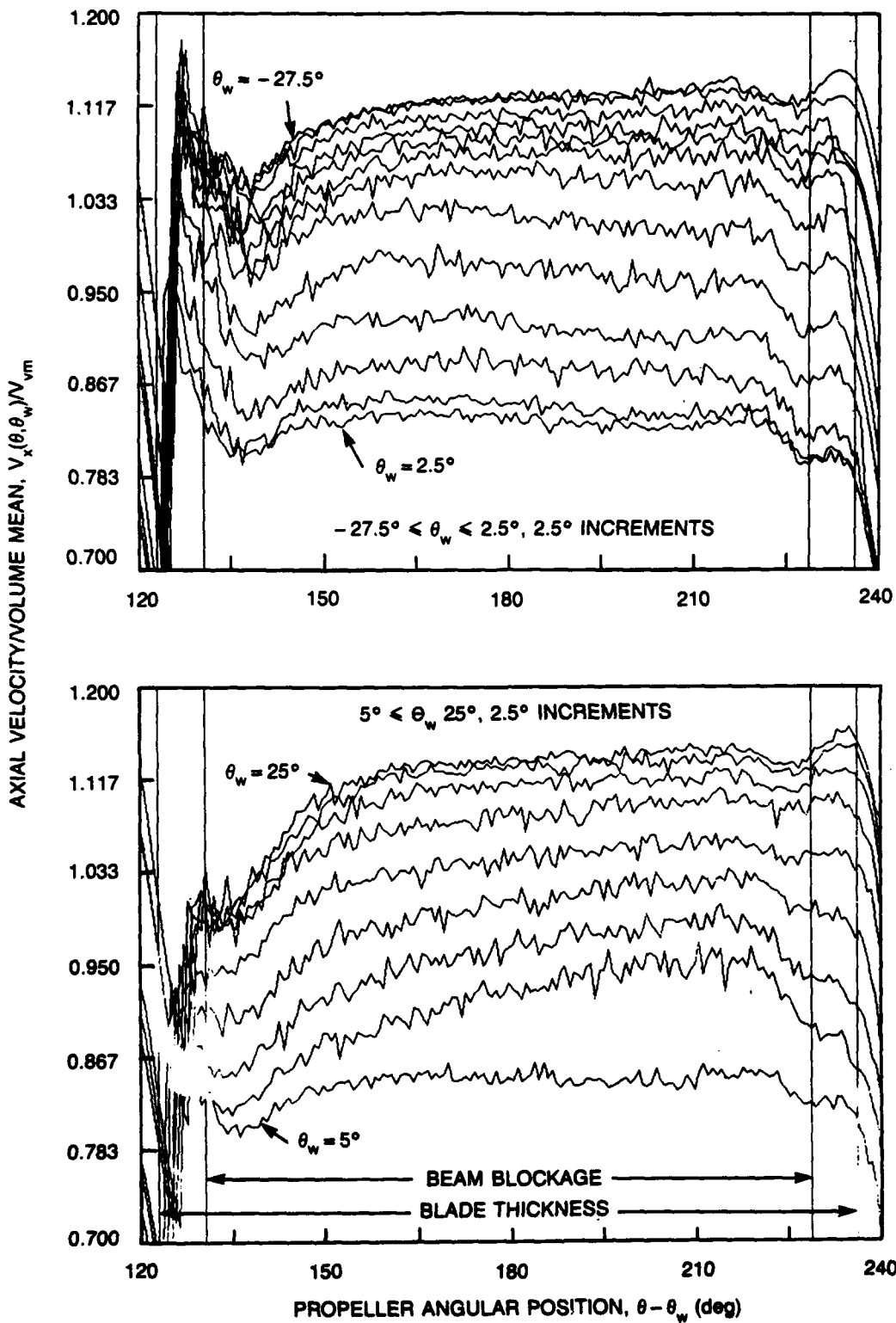


Fig. 21. Variation of effective wake axial velocity at propeller plane.

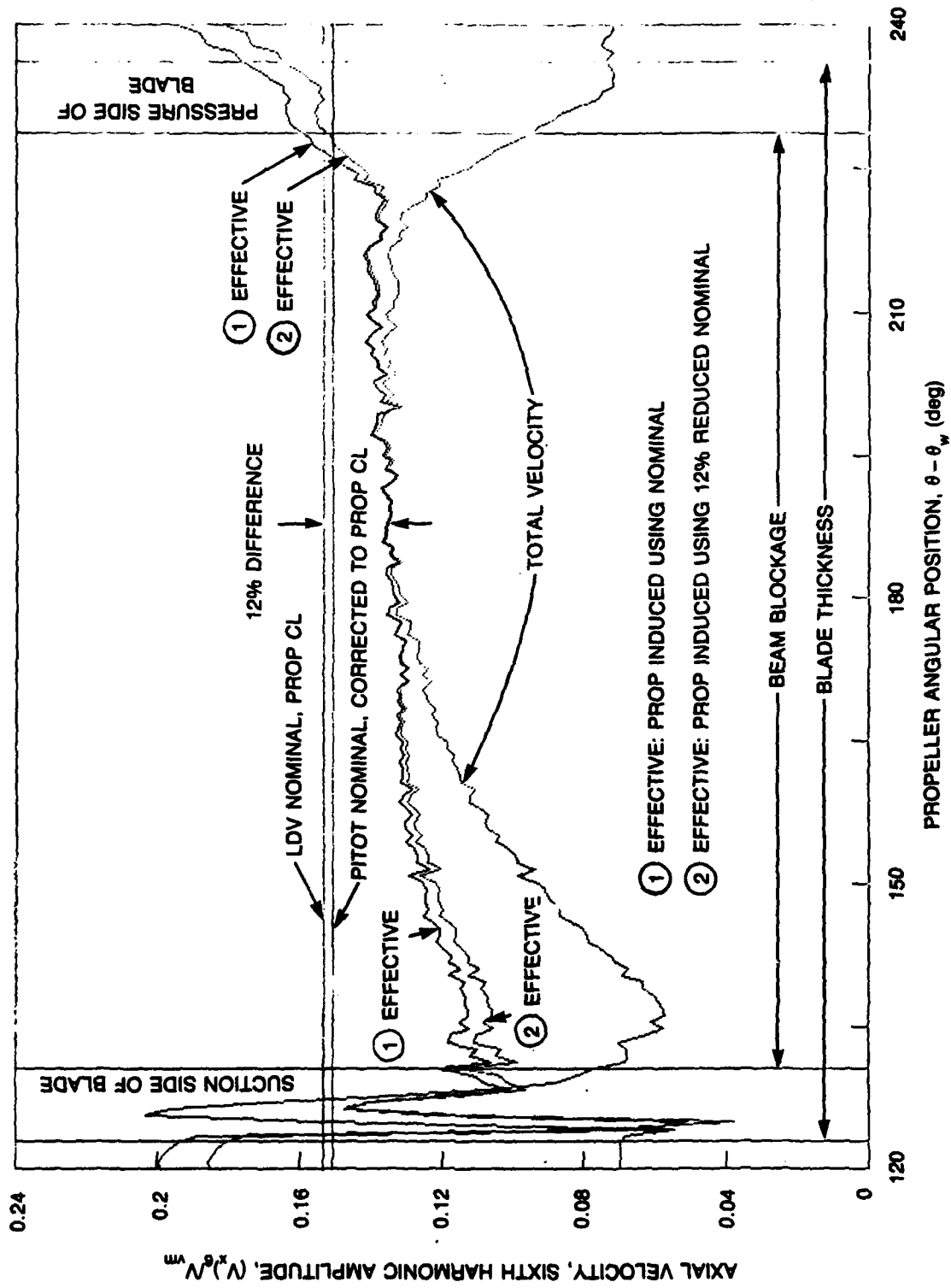


Fig. 22. Variation of measured sixth harmonic wake amplitude at propeller plane.

Table 1. Geometry of DTRC model propellers 4119 and 4132.

Diameter, D : 1.000 ft (0.305m)

Rotation, Right Hand

Number of Blades, : 3

Hub-Diameter Ratio, D_h/D : 0.20

Skew, Rake : None

Design Advance Coefficient, J : 0.833

Section thickness form: NACA66 (DTRC Modified)

Section Mean Line : NACA, $a = 0.8$

Propeller 4119					Propeller 4132			
r/R	c/D	P/D	t/c	f/c	c/D	P/D	t/c	f/c
0.2	0.320	1.105	0.20550	0.01429	0.1600	1.0701	0.2906	0.0240
0.3	0.3625	1.102	0.15530	0.02318	0.1818	1.0925	0.2195	0.0385
0.4	0.4048	1.098	0.11800	0.02303	0.2024	1.0936	0.1670	0.0391
0.5	0.4392	1.093	0.09016	0.02182	0.2196	1.0911	0.1275	0.0357
0.6	0.4610	1.088	0.06960	0.02072	0.2305	1.0883	0.0985	0.0325
0.7	0.4622	1.084	0.5418	0.02003	0.2311	1.0861	0.0766	0.0299
0.8	0.4347	1.081	0.04206	0.01967	0.2173	1.0848	0.0594	0.0280
0.9	0.3613	1.079	0.03321	0.01817	0.1806	1.0838	0.0471	0.0268
0.95	0.2775	1.077	0.03228	0.01631	0.1386	1.0836	0.0455	0.0288
1.0	0.0	1.075	0.03160	0.01175	0	1.0867	0	0

Table 2. Harmonic content of axial velocity generated by wake screens, nondimensionalized by volume mean velocity.

Table 2a. Three-cycle screens.

RADIUS=0.3 MEAN = 0.875

N	A	B	C	PHASE
1	0.01828	0.03596	0.04034	63.1
2	-0.02234	0.00992	0.02444	156.1
3	-0.08973	0.03154	0.09511	160.6
4	-0.00526	-0.00526	0.00743	-135.0
5	0.00454	-0.00179	0.00488	-21.5
6	-0.00275	-0.00167	0.00322	-148.7
7	0.00119	0.00131	0.00178	47.7
8	-0.00191	0.00024	0.00193	172.9
9	-0.00370	0.00036	0.00372	174.5
10	0.00143	-0.00096	0.00172	-33.7
11	-0.00012	-0.00024	0.00027	-116.6
12	-0.00143	-0.00072	0.00160	-153.4
13	0.00119	-0.00131	0.00178	-47.7
14	-0.00036	0.00227	0.00230	99.0
15	0.00036	0.00072	0.00080	63.4

RADIUS=0.5 MEAN = 0.971

N	A	B	C	PHASE
1	-0.00131	0.03106	0.03109	92.4
2	-0.01565	-0.00382	0.01611	-166.3
3	-0.16117	0.04683	0.16784	163.8
4	-0.01900	-0.01744	0.02579	-137.4
5	0.02282	-0.00526	0.02342	-13.0
6	0.02127	0.00084	0.02128	2.3
7	-0.00944	0.01183	0.01513	128.6
8	-0.01302	-0.00514	0.01400	-158.5
9	-0.02700	0.02186	0.03474	141.0
10	0.00251	-0.00992	0.01023	-75.8
11	-0.00155	-0.00609	0.00629	-104.3
12	-0.00215	0.00299	0.00368	125.8
13	0.00490	-0.00215	0.00535	-23.7
14	-0.00358	-0.00108	0.00374	-163.3
15	-0.00036	0.00346	0.00348	95.9

RADIUS=0.7 MEAN = 1.005

N	A	B	C	PHASE
1	0.01386	0.02282	0.02670	58.7
2	-0.02162	-0.00167	0.02169	-175.6
3	-0.16428	0.04337	0.16991	165.2
4	-0.01995	0.00562	0.02073	164.3
5	0.00538	-0.00323	0.00627	-31.0
6	0.03011	-0.02270	0.03771	-37.0
7	0.00072	-0.01207	0.01209	-86.6
8	-0.00454	-0.00084	0.00462	-169.6
9	-0.02855	0.02222	0.03618	142.1
10	-0.00072	-0.00908	0.00911	-94.5
11	-0.00836	0.00311	0.00892	159.6
12	-0.00406	0.01350	0.01410	106.7
13	-0.00430	-0.00526	0.00679	-129.3
14	-0.00108	-0.00789	0.00796	-97.8
15	0.00024	-0.00191	0.00193	-82.9

RADIUS=0.9 MEAN = 1.045

N	A	B	C	PHASE
1	-0.01326	0.02784	0.03084	115.5
2	0.00155	-0.01075	0.01086	-81.8
3	-0.19654	0.06798	0.20796	160.9
4	-0.00693	-0.00466	0.00835	-146.1
5	0.00119	0.01529	0.01534	85.5
6	0.03262	-0.02270	0.03974	-34.8
7	0.00836	-0.00765	0.01133	-42.4
8	-0.00753	0.00860	0.01143	131.2
9	-0.02389	0.02079	0.03167	139.0
10	-0.01051	-0.00490	0.01160	-155.0
11	-0.01314	0.00418	0.01379	162.3
12	-0.00442	0.02915	0.02948	98.6
13	-0.00490	-0.00765	0.00908	-122.6
14	0.00060	0.00323	0.00328	79.5
15	-0.00108	-0.01517	0.01521	-94.1

Table 2. (Continued)

Table 2b. Six-cycle screens.

RADIUS=0.3 MEAN = 1.001

N	A	B	C	PHASE
1	-0.00857	0.01304	.01561	123.3
2	-0.00942	0.00205	0.00964	167.7
3	-0.01751	0.00097	0.01754	176.8
4	0.00918	-0.00580	0.01085	-32.3
5	0.01437	-0.00495	0.01520	-19.0
6	-0.01256	0.00386	0.01314	162.9
7	-0.00048	-0.00374	0.00377	-97.4
8	0.00024	0.00012	0.00027	26.6
9	0.00024	0.00024	0.00034	45.0
10	0.00072	0.00072	0.00102	45.0
11	-0.00036	0.00036	0.00051	135.0
12	0.00012	-0.00036	0.00038	-71.6
13	-0.00024	0.00000	0.00024	180.0
14	0.00048	0.00060	0.00077	51.3
15	-0.00072	0.00109	0.00131	123.7

RADIUS=0.5 MEAN = 0.970

N	A	B	C	PHASE
1	0.00990	0.01473	0.01775	56.1
2	0.03864	0.02874	0.04816	36.6
3	-0.00399	-0.00664	0.00775	-121.0
4	-0.00978	-0.00555	0.01125	-150.4
5	0.03502	-0.03043	0.04639	-41.0
6	-0.09794	0.01449	0.09900	171.6
7	-0.01739	-0.02633	0.03155	-123.4
8	0.00193	-0.01075	0.01092	-79.8
9	0.00060	-0.01389	0.01390	-87.5
10	-0.00205	0.00833	0.00858	103.8
11	-0.00411	0.00157	0.00440	159.1
12	0.00290	-0.00193	0.00348	-33.7
13	0.00024	0.00169	0.00171	81.9
14	0.00097	-0.00435	0.00445	-77.5
15	-0.00097	0.00290	0.00305	108.4

RADIUS=0.7 MEAN = 1.018

N	A	B	C	PHASE
1	-0.00737	0.00580	0.00937	141.8
2	0.01111	-0.01509	0.01874	-53.6
3	0.01365	-0.02162	0.02556	-57.7
4	-0.02922	0.01534	0.03300	152.3
5	-0.01485	0.01135	0.01869	142.6
6	-0.15203	0.04408	0.15830	163.8
7	0.02294	-0.02029	0.03063	-41.5
8	-0.00749	0.00242	0.00787	162.1
9	-0.00278	-0.00109	0.00298	-158.6
10	-0.00507	-0.01497	0.01581	-108.7
11	-0.01123	0.01051	0.01538	136.9
12	-0.03103	0.03188	0.04449	134.2
13	0.01679	-0.00869	0.01890	-27.4
14	-0.00507	0.00906	0.01038	119.2
15	0.00229	-0.00133	0.00265	-30.1

RADIUS=0.9 MEAN = 1.007

N	A	B	C	PHASE
1	0.00555	-0.00254	0.00611	-24.5
2	-0.02174	-0.00048	0.02174	-178.7
3	0.00133	0.00906	0.00915	81.7
4	-0.01111	0.01183	0.01623	133.2
5	-0.00471	0.04057	0.04085	96.6
6	-0.20952	0.07958	0.22412	159.2
7	0.02862	0.00060	0.02863	1.2
8	-0.01171	0.00809	0.01424	145.4
9	0.01413	0.00000	0.01413	0.0
10	0.00761	-0.01352	0.01552	-60.6
11	-0.00749	0.01485	0.01663	116.8
12	-0.02319	0.03550	0.04240	123.1
13	0.01208	-0.00519	0.01314	-23.3
14	-0.00242	-0.00060	0.00249	-166.0
15	0.00000	-0.00652	0.00652	-90.0

Table 2. (Continued)

Table 2c. Nine-cycle screens.

RADIUS=0.3 MEAN = 0.983

N	A	B	C	PHASE
1	-0.00903	0.00903	0.01276	135.0
2	0.00505	0.00638	0.00814	51.6
3	-0.00156	-0.00566	0.00587	-105.5
4	-0.00554	-0.00024	0.00554	-177.5
5	-0.00036	0.00457	0.00459	94.5
6	-0.00060	-0.00084	0.00104	-125.5
7	0.00096	0.00108	0.00145	48.4
8	0.00036	0.00000	0.00036	0.0
9	-0.00036	-0.00036	0.00051	-135.0
10	-0.00036	-0.00084	0.00092	-113.2
11	0.00048	-0.00024	0.00054	-26.6
12	0.00036	0.00012	0.00038	18.4
13	0.00024	0.00036	0.00043	56.3
14	-0.00024	0.00036	0.00043	123.7
15	0.00024	0.00024	0.00034	45.0

RADIUS=0.5 MEAN = 0.996

N	A	B	C	PHASE
1	0.00277	0.02696	0.02710	84.1
2	-0.00361	0.01179	0.01233	107.0
3	-0.00890	0.01324	0.01595	123.9
4	-0.02274	0.00132	0.02278	176.7
5	0.01649	0.02587	0.03068	57.5
6	0.02623	-0.00602	0.02691	-12.9
7	0.01191	0.01829	0.02183	56.9
8	0.00638	-0.00794	0.01019	-51.2
9	-0.02250	0.00181	0.02258	175.4
10	-0.00084	-0.00794	0.00799	-96.1
11	0.00493	-0.00144	0.00514	-16.3
12	0.00205	-0.00181	0.00273	-41.4
13	0.00108	-0.00590	0.00600	-79.6
14	0.00132	0.00000	0.00132	0.0
15	-0.00060	-0.00060	0.00085	-135.0

RADIUS=0.7 MEAN = 1.005

N	A	B	C	PHASE
1	-0.01264	-0.00590	0.01394	-155.0
2	-0.01372	0.00866	0.01623	147.7
3	0.01215	-0.00830	0.01472	-34.3
4	0.00024	0.00806	0.00807	88.3
5	-0.00277	-0.01384	0.01411	-101.3
6	-0.01143	-0.01396	0.01804	-129.3
7	0.00614	-0.00217	0.00651	-19.4
8	0.05174	0.02912	0.05938	29.4
9	-0.08821	0.02010	0.09047	167.2
10	-0.02671	0.02972	0.03996	131.9
11	0.01107	-0.01143	0.01591	-45.9
12	0.00698	0.00385	0.00797	28.9
13	0.00289	-0.02515	0.02532	-83.4
14	-0.00445	-0.00361	0.00573	-141.0
15	-0.00481	-0.00313	0.00574	-147.0

RADIUS=0.9 MEAN = 1.005

N	A	B	C	PHASE
1	-0.00529	-0.00409	0.00669	-142.3
2	0.01528	0.00806	0.01728	27.8
3	0.01059	0.01745	0.02041	58.7
4	0.00445	0.01059	0.01149	67.2
5	-0.01372	-0.00277	0.01399	-168.6
6	-0.01986	-0.01083	0.02262	-151.4
7	0.03815	-0.00734	0.03885	-10.9
8	0.05596	0.03983	0.06869	35.4
9	-0.15620	0.03261	0.15957	168.2
10	-0.01588	0.03947	0.04255	111.9
11	-0.02094	0.00770	0.02231	159.8
12	0.00397	0.00614	0.00731	57.1
13	0.00108	-0.01324	0.01328	-85.3
14	-0.00782	-0.00734	0.01073	-136.8
15	-0.00397	0.00036	0.00399	174.8

Table 2. (Continued)

Table 2d. Twelve-cycle screens.

RADIUS=0.3 MEAN = 0.942

N	A	B	C	PHASE
1	-0.01376	0.00347	0.01419	165.8
2	-0.01628	-0.01137	0.01985	-145.1
3	0.00802	0.00610	0.01008	37.3
4	-0.00299	0.00658	0.00723	114.4
5	0.00251	0.00215	0.00331	40.6
6	-0.00191	-0.00012	0.00192	-176.4
7	-0.00180	0.00048	0.00186	165.1
8	-0.00036	-0.00024	0.00043	-146.3
9	0.00072	0.00036	0.00080	26.6
10	0.00024	0.00048	0.00054	63.4
11	0.00012	0.00000	0.00012	0.0
12	0.00024	-0.00060	0.00064	-68.2
13	0.00048	-0.00024	0.00054	-26.6
14	0.00000	-0.00048	0.00048	-90.0
15	-0.00012	-0.00036	0.00038	-108.4

RADIUS=0.5 MEAN = 0.976

N	A	B	C	PHASE
1	-0.00012	0.02058	0.02058	90.3
2	-0.00921	-0.00742	0.01183	-141.2
3	-0.00048	0.00562	0.00565	94.9
4	-0.00718	0.00682	0.00990	136.5
5	-0.00227	-0.00132	0.00263	-149.9
6	0.00096	0.00766	0.00772	82.9
7	-0.00694	-0.00527	0.00871	-142.8
8	0.00610	0.00598	0.00855	44.4
9	-0.00347	0.00048	0.00350	172.1
10	0.00036	0.00012	0.00038	18.4
11	0.00347	0.00096	0.00360	15.4
12	-0.00048	-0.00598	0.00600	-94.6
13	0.00562	0.00144	0.00581	14.3
14	0.00024	-0.00036	0.00043	-56.3
15	-0.00024	0.00012	0.00027	153.4

RADIUS=0.7 MEAN = 1.027

N	A	B	C	PHASE
1	0.00311	0.01041	0.01087	73.4
2	0.00455	0.00933	0.01038	64.0
3	-0.00072	-0.00694	0.00698	-95.9
4	-0.00754	-0.01675	0.01837	-114.2
5	-0.00215	0.00694	0.00727	107.2
6	0.00012	0.01173	0.01173	89.4
7	0.01508	-0.00742	0.01681	-26.2
8	0.00467	0.00790	0.00917	59.4
9	0.01089	-0.01556	0.01899	-55.0
10	0.00012	0.00862	0.00862	89.2
11	-0.02166	0.01747	0.02783	141.1
12	-0.04727	-0.01723	0.05031	-160.0
13	0.01364	0.01257	0.01855	42.6
14	-0.00227	-0.00287	0.00366	-128.4
15	0.00144	0.00443	0.00466	72.0

RADIUS=0.9 MEAN = 1.012

N	A	B	C	PHASE
1	0.00371	0.00778	0.00862	64.5
2	-0.00144	-0.00419	0.00443	-108.9
3	-0.00886	-0.00024	0.00886	-178.5
4	0.00874	-0.00132	0.00883	-8.6
5	0.00562	-0.00515	0.00762	-42.5
6	-0.00060	-0.00239	0.00247	-104.0
7	0.00933	-0.00383	0.01009	-22.3
8	0.00562	0.00551	0.00787	44.4
9	0.00874	-0.00263	0.00912	-16.8
10	-0.00467	0.01484	0.01556	107.5
11	-0.04871	0.03854	0.06211	141.7
12	-0.09670	-0.04464	0.10650	-155.2
13	0.01867	0.03076	0.03598	58.7
14	-0.01173	-0.00838	0.01441	-144.5
15	0.00024	0.00072	0.00076	71.6

Table 3. Unsteady thrust and torque.

Table 3a. Three-cycle screens.

3 CYCLE SCREEN J=0.833 AMP=1000*THRUST OR TORQUE COEFFICIENT

N	PROPELLER 4132				PROPELLER 4119			
	THRUST		TORQUE		THRUST		TORQUE	
	AMP	PHASE	AMP	PHASE	AMP	PHASE	AMP	PHASE
0	153.93	0.0	27.78	0.0	153.61	0.0	29.28	0.0
3	41.32	-26.3	5.48	-29.7	51.61	-77.9	7.65	-79.8
6	6.33	106.3	1.21	103.2	6.23	12.3	1.25	9.4
9	4.50	-97.6	0.77	-97.4	1.29	82.2	0.28	90.6
12	2.46	-137.5	0.33	-139.5	1.19	-0.4	0.25	-8.5

CALCULATED THRUST AND TORQUE USING PUF-2

3 CYCLE SCREEN J=0.833 AMP=1000*THRUST OR TORQUE COEFFICIENT

N	PROPELLER 4132				PROPELLER 4119			
	THRUST		TORQUE		THRUST		TORQUE	
	AMP	PHASE	AMP	PHASE	AMP	PHASE	AMP	PHASE
0	152.62	0.0	27.03	0.0	155.36	0.0	29.14	0.0
3	43.27	-42.0	6.15	-51.6	60.75	-87.8	10.06	-91.7
6	6.99	87.8	1.23	83.0	6.61	19.0	1.18	22.4
9	5.32	-132.2	0.95	-131.1	3.43	83.3	0.57	85.1
12	2.12	178.5	0.32	-179.6	0.57	85.8	0.09	101.3

RATIO OF AMPS AND DIF OF PHASES

3 CYCLE SCREEN J=0.833 AMP=1000*THRUST OR TORQUE COEFFICIENT

N	PROPELLER 4132				PROPELLER 4119			
	THRUST		TORQUE		THRUST		TORQUE	
	C/M AMP	C-M PHASE	C/M AMP	C-M PHASE	C/M AMP	C-M PHASE	C/M AMP	C-M PHASE
0	0.99	0.0	0.97	0.0	1.01	0.0	1.00	0.0
3	1.05	-15.7	1.12	-21.9	1.18	-9.8	1.32	-11.9
6	1.10	-18.5	1.01	-20.2	1.06	6.7	0.94	13.0
9	1.18	-34.7	1.24	-33.7	2.65	1.1	2.00	-5.5
12	0.86	316.0	0.96	-40.1	0.48	86.2	0.37	109.9

Table 3. (Continued)

Table 3b. Six-cycle screens.

6 CYCLE SCREEN J=0.833 AMP=1000*THRUST OR TORQUE COEFFICIENT

N	PROPELLER 4132		PROPELLER 4119		PROPELLER 4132		PROPELLER 4119	
	THRUST AMP	PHASE	TORQUE AMP	PHASE	THRUST AMP	PHASE	TORQUE AMP	PHASE
0	154.63	0.0	27.34	0.0	153.49	0.0	29.52	0.0
3	2.16	104.2	0.29	103.6	1.98	59.5	0.27	60.4
6	30.58	-78.8	4.24	-81.3	23.16	-141.9	3.44	-138.4
9	0.14	-12.0	0.02	-94.6	0.84	102.1	0.13	101.7
12	3.33	-178.5	0.39	170.8	2.46	1.8	0.43	-10.9

CALCULATED THRUST AND TORQUE USING PUF-2

6 CYCLE SCREEN J=0.833 AMP=1000*THRUST OR TORQUE COEFFICIENT

N	PROPELLER 4132		PROPELLER 4119		PROPELLER 4132		PROPELLER 4119	
	THRUST AMP	PHASE	TORQUE AMP	PHASE	THRUST AMP	PHASE	TORQUE AMP	PHASE
0	153.53	0.0	27.23	0.0	156.03	0.0	29.29	0.0
3	1.84	88.9	0.22	73.8	2.48	32.2	0.41	21.2
6	34.30	-77.2	5.51	-84.3	30.64	-140.0	4.80	-137.7
9	0.53	98.9	0.09	75.2	1.07	89.3	0.16	96.0
12	3.76	-160.7	0.55	-157.6	1.01	71.2	0.15	88.8

RATIO OF AMPS AND DIF OF PHASES

6 CYCLE SCREEN J=0.833 AMP=1000*THRUST OR TORQUE COEFFICIENT

N	PROPELLER 4132		PROPELLER 4119		PROPELLER 4132		PROPELLER 4119	
	THRUST C/M AMP	C-M PHASE	TORQUE C/M AMP	C-M PHASE	THRUST C/M AMP	C-M PHASE	TORQUE C/M AMP	C-M PHASE
0	0.99	0.0	1.00	0.0	1.02	0.0	0.99	0.0
3	0.85	-15.3	0.76	-29.8	1.25	-27.3	1.50	-39.2
6	1.12	1.6	1.30	-3.0	1.32	1.9	1.39	0.7
9	3.69	110.9	3.78	169.9	1.28	-12.8	1.20	-5.7
12	1.13	17.8	1.42	-328.4	0.41	69.4	0.36	99.7

Table 3. (Continued)

Table 3c. Nine-cycle screens.

9 CYCLE SCREEN J=0.833 AMP=1000*THRUST OR TORQUE COEFFICIENT

N	PROPELLER 4132				PROPELLER 4119			
	THRUST		TORQUE		THRUST		TORQUE	
	AMP	PHASE	AMP	PHASE	AMP	PHASE	AMP	PHASE
0	149.85	0.0	27.62	0.0	154.46	0.0	30.16	0.0
3	2.83	-170.8	0.39	-173.6	3.32	175.1	0.52	175.5
6	2.27	-9.4	0.30	-14.0	2.96	-82.6	0.43	-85.4
9	14.99	-99.1	2.26	-101.4	6.40	164.0	0.99	154.7
12	0.40	129.5	0.05	144.5	0.26	-57.7	0.04	-39.4

CALCULATED THRUST AND TORQUE USING PUF -2

9 CYCLE SCREEN J=0.833 AMP=1000*THRUST OR TORQUE COEFFICIENT

N	PROPELLER 4132				PROPELLER 4119			
	THRUST		TORQUE		THRUST		TORQUE	
	AMP	PHASE	AMP	PHASE	AMP	PHASE	AMP	PHASE
0	153.49	0.0	27.25	0.0	155.98	0.0	29.29	0.0
3	1.93	-162.0	0.26	-164.0	2.63	161.2	0.39	159.6
6	3.24	5.0	0.51	5.8	4.66	-72.0	0.73	-71.9
9	17.52	-91.8	3.14	-94.5	8.58	162.7	1.28	162.4
12	0.47	126.1	0.08	133.9	0.31	56.8	.06	54.6

RATIO OF AMPS AND DIF OF PHASES

9 CYCLE SCREEN J=0.833 AMP=1000*THRUST OR TORQUE COEFFICIENT

N	PROPELLER 4132				PROPELLER 4119			
	THRUST		TORQUE		THRUST		TORQUE	
	C/M AMP	C-M PHASE	C/M AMP	C-M PHASE	C/M AMP	C-M PHASE	C/M AMP	C-M PHASE
0	1.02	0.0	0.99	0.0	1.01	0.0	0.97	0.0
3	0.68	8.8	0.66	9.6	0.79	-13.9	0.75	-15.9
6	1.43	14.4	1.71	19.9	1.57	10.6	1.67	13.5
9	1.17	7.3	1.39	6.9	1.34	-1.3	1.29	7.7
12	1.17	-3.4	1.69	-10.6	1.21	114.5	1.61	94.0

Table 3. (Continued)

Table 3d. Twelve-cycle screens.

MEASURED THRUST AND TORQUE

12 CYCLE SCREEN J=0.833 AMP=1000*THRUST OR TORQUE COEFFICIENT

N	PROPELLER 4132		PROPELLER 4119		PROPELLER 4132		PROPELLER 4119	
	THRUST AMP	PHASE	TORQUE AMP	PHASE	THRUST AMP	PHASE	TORQUE AMP	PHASE
0	151.84	0.0	27.92	0.0	151.99	0.0	29.70	0.0
3	0.69	-5.2	0.08	-1.1	0.51	-22.8	0.05	-15.3
6	0.91	169.0	0.13	164.5	0.86	98.4	0.15	102.9
9	1.64	38.9	0.25	34.9	1.49	-57.1	0.27	-56.5
12	7.10	-77.1	1.07	-76.9	2.63	141.2	0.61	133.9

CALCULATED THRUST AND TORQUE USING PUF-2

12 CYCLE SCREEN J=0.833 AMP=1000*THRUST OR TORQUE COEFFICIENT

N	PROPELLER 4132		PROPELLER 4119		PROPELLER 4132		PROPELLER 4119	
	THRUST AMP	PHASE	TORQUE AMP	PHASE	THRUST AMP	PHASE	TORQUE AMP	PHASE
0	152.65	0.0	27.14	0.0	155.14	0.0	29.17	0.0
3	0.71	6.2	0.08	14.5	0.99	-23.7	0.13	-24.5
6	1.20	-166.4	0.22	-170.8	0.95	87.3	0.13	90.2
9	1.59	48.6	0.28	46.1	1.11	-114.9	0.18	-117.0
12	7.61	-75.4	1.25	-73.6	2.27	-169.6	0.38	-162.2

RATIO OF AMPS AND DIF OF PHASES

12 CYCLE SCREEN J=0.833 AMP=1000*THRUST OR TORQUE COEFFICIENT

N	PROPELLER 4132		PROPELLER 4119		PROPELLER 4132		PROPELLER 4119	
	THRUST C/M AMP	C-M PHASE	TORQUE C/M AMP	C-M PHASE	THRUST C/M AMP	C-M PHASE	TORQUE C/M AMP	C-M PHASE
0	1.01	0.0	0.97	0.0	1.02	0.0	0.98	0.0
3	1.02	11.4	1.02	15.6	1.94	-0.9	2.72	-9.2
6	1.33	-335.4	1.67	-335.3	1.10	-11.1	0.90	-12.7
9	0.97	9.7	1.09	11.2	0.75	-57.8	0.65	-60.5
12	1.07	1.7	1.17	3.3	0.86	-310.8	0.63	-296.1

REFERENCES

1. Boswell, R.J. and M.L. Miller, "Unsteady Propeller Loading-Measurement, Correlation With Theory, and Parametric Study," Naval Ship Research and Development Center Report 2625 (Oct 1968).
2. Boswell, R.J. et al., "Practical Methods for Predicting Periodic Propeller Loads," Second International Symposium on Practical Design in Shipbuilding (PRADS 83), Tokyo, Japan/Seoul, Korea (Oct 1983), also DTNSRDC Report 83/090 (Oct 1983).
3. Kerwin, J.E. and C.S. Lee, "Prediction of Steady and Unsteady Marine Propeller Performance by Numerical Lifting Surface Theory," Transactions SNAME, Vol. 86, pp. 218-253 (1978).
4. Tsakonas, S. et al., "An Exact Linear Lifting Surface Theory for Marine Propellers in a Nonuniform Flow Field," Journal of Ship Research, Vol. 17, No. 4, pp. 196-207 (1974).
5. Huang, T.T. and N.C. Groves, "Effective Wake: Theory and Experiment," 13th Symposium on Naval Hydrodynamics, Tokyo, Japan (1980), also DTNSRDC Report 81/033 (1981).
6. Breslin, J.P. et al., "Theoretical and Experimental Propeller-Induced Hull Pressures Arising from Intermittent Blade Cavitation, Loading, and Thickness," Transactions SNAME, Vol. 90, pp. 111-151 (1982).
7. Miller, M.L., "Experimental Determination of Unsteady Propeller Forces," 7th Symposium on Naval Hydrodynamics, Rome, Italy (1968).
8. Jessup, S.D. et al., "Local Propeller Blade Flows in Uniform and Sheared Onset Flows Using LDV Techniques," 15th Symposium on Naval Hydrodynamics, Hamburg, Germany (1984).
9. Brooks, J.E., "Vibrations of a Marine Propeller Operating in a Nonuniform Inflow," DTNSRDC Report 80/056 (Apr 1980).

THIS PAGE INTENTIONALLY LEFT BLANK

INITIAL DISTRIBUTION

Copies	Copies
1 Army Chief of Res & Dev	NAVSEA (Continued)
1 AER&DL	1 SEA 56XN
4 CHONR	1 PMS-383
1 Lib	1 PMS-392
1 Code 11	1 PMS-396
1 Code 21	1 PMS-399
1 Code 12	1 PMS-400
4 ONR Boston	1 SEA Tech Rep
4 ONR Chicago	Bath, England
4 ONR London, England	2 DET Norfolk (Sec 6660)
1 NRL	2 MMA
2 USNA	1 Lib
1 Lib	1 Maritime Res Cen
1 Johnson	12 DTIC
1 NAVPGSCOL Lib	2 HQS COGARD
1 NROTC & NAVADMINU, MIT	1 US Coast Guard (G-ENE-4A)
1 NADC	1 LC/SCI & Tech Div
4 NOSC	2 NASA STIF
1 1311 Lib	1 Dir Res
1 6005	1 NSF Engr Div/Lib
1 13111 Lib	1 DOT Lib
1 Mautner	2 U. Cal Berkeley/Dept Name
1 NSWC	1 Name Lib
31 NAVSEA	1 Webster
5 SEA 05R	1 U. Mississippi Dept of M.E.
1 SEA 55	1 Fox
3 SEA 55N	3 CIT
1 SEA 55W	1 AERO Lib
3 SEA 56D	1 Acosta
1 SEA 56X	1 Wu
3 SEA 56X1	4 U. Iowa
1 SEA 56X2	1 Lib
3 SEA 56X7	1 IHR/Kennedy
1 SEA 56X5	1 IHR/Stern
	1 IHR/Patel

INITIAL DISTRIBUTION (Continued)

Copies		Copies	
3	U. Michigan/Dept Name 1 Name Lib 1 Parsons 1 Vorus	1	WHOI Ocean Engr Dept
3	MIT 1 Barker Engr Lib 2 Ocean Engr/Kerwin	1	WPI Alden Hydr Lab Lib
3	State U Maritime Coll 1 ARL Lib 1 Engr Dept 1 Inst Math Sci	1	ASME/Res Comm Info
4	Penn State U ARL 1 Lib 1 Henderson 1 Gearhart 1 Thompson	1	ASNE
1	Boeing Adv Amr Sys Div	1	SNAME/Tech Lib
1	BB&N/Jackson	1	AERO Jet-General/Beckwith
1	Brewer Engr Lab	1	Allis Chalmers, York, PA
1	Cambridge Acous/Junger	1	AVCO Lycoming
1	Calspan, Inc/Ritter	1	Baker Manufacturing
1	Stanford U/Ashley	1	Bird-Johnson Co/Norton
1	Stanford Res Inst Lib	1	Douglas Aircraft/Lib
2	Sit Davidson Lab 1 Lib 1 Savitski	2	Exxon Res Div 1 Lib 1 Fitzgerald
1	Texas U ARL Lib	1	Friede & Goldman/Michel
1	Utah State U/Jeppson	1	General Dynamics, EB/Boatwright
2	VPI/Dept Aero & Ocean Engr 1 Schetz 1 Kaplan	1	Gibbs & Cox/Lib
2	Webb Inst 1 Ward 1 Hadler	1	Rosenblatt & Son/Lib
		1	Grumman Aerospace/Carl
		1	Tracor Hydronautics/Lib
		1	Ingalls Shipbuilding
		1	Inst for Defense Anal
		1	Itek Vidya
		1	Lips Duran/Kress
		1	Littleton R & Engr Corp/Reed

